Studies on Decomposition Catalysts for Hazardous Organic Compounds from Wastewater by Using Oxides with Rare Earth

(希土類含有酸化物を用いた排水中における有害有機酸化物の分解触媒に関する研究)

Pil Gyu Choi

2017

Division of Applied Chemistry
Graduate School of Engineering
Osaka University

Preface

The work of this thesis has been carried out under the supervision of Professor Dr. Nobuhito Imanaka at Division of Applied Chemistry, Graduate School of Engineering, Osaka University.

The object of this thesis is to develop novel environmental catalysts for removal of hazardous organic compounds from wastewater at moderate condition.

The author wishes that the findings of this study provide useful suggestions and information for further development and establishment of novel environmental catalysts and that the materials would contribute to more practical applications.

Pil Gyu Choi

Divition of Applied Chemistry

Graduate School of Engineering

Osaka University

2-1Yamadaoka, Suita Osaka 565-0871

Japan

January 2017

Contents

General Introduction

During the high-level development of chemical industry in the past decades, industrial wastewater has caused a major environmental contamination according to an increase in the amount of chemical substances and water consumption. Especially, industrial liquid waste from chemical industry contains organic compounds [1], used as a solvent and an intermediate for synthesis of products; for instance, acetaldehyde, 1,4-dioxane, and bisphenol-A. These organic compounds lead to several problems for human health and the environment due to their toxicity, carcinogenicity, and endocrine modulatory effects [1-5]. Therefore, to protect our health and the environment, hazardous organic compounds have been stringently regulated and monitored based on water pollution control law and PRTR (pollutant release and transfer register) regulation [5, 6]. Accordingly, development of effective removal processes is required to remove these organic compounds from wastewater as much as possible.

In general, the conventional water treatment processes, including activated carbon treatment, coagulating sedimentation process, and process for using microorganism, have been mainly used to remove the hazardous organic compounds of wastewater. However, these processes exhibit low efficiency for the high concentration and refractory organic compounds [7-9]. Also, these processes have problems, such as replacement of activated carbon, post-treatment of sediments, and control of pH and temperature for microorganisms. Recently, advanced oxidation processes were studied using strongly oxidizing agents (H_2O_2 or O_3) [10-15] and UV irradiation [16-20], and they exhibited appreciable removal efficiency. However, they require constant supply of hazardous oxidizing additives or UV irradiation. Meanwhile, some particular degrading bacteria have been reported in spite of high resistance to biodegradation of refractory hazardous organic compounds. According to K. Sei et al. [21], biodegradation performance for refractory 1,4-dioxane reached a high removal rate

of 50%. This process, however, requires not only a long reaction time (70-80 h) but also the satisfaction of biochemical oxygen demand. These problems show that there still remains a need to overcome the requirement for strict reaction conditions.

On the other hand, catalytic decomposition method can oxidize refractory and hazardous organic compounds in liquid phase in a short reaction time without the supply of any additives or light irradiation. Especially, the use of heterogeneous catalyst gives benefits; easy separation of the catalyst and the liquid reactants, readily-recoverable of the catalysis by calcination, and reaction in a serial manner as compared with homogeneous catalysts [1]. Therefore, catalytic decomposition method using a heterogeneous catalyst is expected as a practically applicable method. As an example, $Ag/CeO_2–ZrO_2$ (Ag/CZ) catalyst has been reported to exhibited a removal property for a refractory hazardous organic compound of bisphenol-A [22]. For this method, however, the high pressure (20 atm) and the high temperature (160°C) were required for the catalytic decomposition in water. Since these requirements of high pressure and high temperature are not favorable from a practical application standpoint, it is necessary to develop novel catalysts with high oxidation activity to remove organic compounds effectively at the moderate condition.

Hence, the present study aims to develop the novel catalysts which can effectively oxidize hazardous organic compounds in water under the moderate reaction condition (under atmospheric pressure and below 100°C). To this end, since the oxidative decomposition is considered to be difficult by using only dissolved oxygen in water, I focused on rare earth oxides that can supply the oxygen to the catalyst from inside the lattice. Figure G-1 shows the diagram of oxygen supply from the rare earth oxide. Normally, oxidation reaction of organic compounds occurs using a dissolved oxygen via adsorption on the catalyst (reaction a). In the case of the rare earth oxide supported catalyst, oxygen is further supplied from inside of the rare earth oxide (reaction b). Additionally, the rare earth oxide stores an oxide ion from a dissolved oxygen (reaction c). Thereby, it is expected that the catalytic oxidation is facilitated by using the rare earth oxide, and the hazardous organic compounds are

effectively removed.

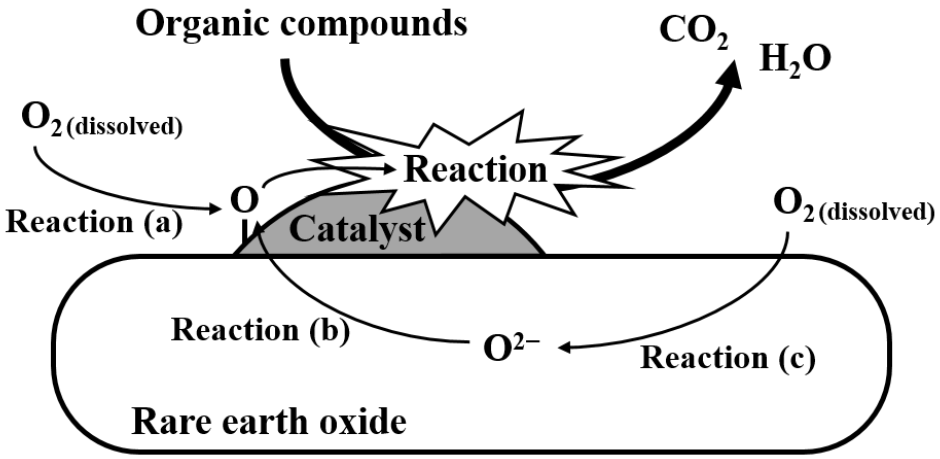

Figure G-1. Diagram of possible oxygen supply for the oxidation reaction on the catalyst supported on the rare earth oxide.

This thesis consists of the following three chapters.

In **Chapter 1**, for the efficient removal of the hazardous organic compounds, CeO_2–ZrO_2–SnO_2 as an oxide with rare earth was selected as a promoter of a platinum (Pt) catalyst. CeO_2–ZrO_2–SnO_2 possesses high oxygen release and storage abilities [23], expecting that an enhancement of the oxygen supplies to the catalyst by acceleration of the oxygen spillover from the promoter [24]. Accordingly, a Pt/CeO_2–ZrO_2–SnO_2/γ-Al_2O_3 catalyst was synthesized, and the catalytic removal performance for the hazardous organic compound of acetaldehyde was investigated.

In **Chapter 2**, I focused on 1,4-dioxane, which is refractory organic compound as compared to acetaldehyde, as the target to be removed by catalysts. For efficient removal of 1,4-dioxane, the surface area of catalysts was further increased by using mesoporous silica SBA-16 (Santa Barbara Amorphous No. 16) as a support to increase the catalytic active sites, and the Pt/CeO_2–ZrO_2–SnO_2/SBA-16 catalyst was synthesized and investigated its catalytic removal performance for 1,4-dioxane. In addition, our group reported that CeO_2–ZrO_2–Bi_2O_3 also possessed high oxygen release and storage abilities [25]. Accordingly, the Pt/CeO_2–ZrO_2–Bi_2O_3/SBA-16 catalyst was also synthesized, and the catalytic removal performance for 1,4-dioxane was investigated.

Combination of SBA-16 having large surface area and CeO_2–ZrO_2–Bi_2O_3 with the high oxygen release and storage abilities has a possibility to realize the oxidation of organic compounds even if Pt is not used as the oxidizing catalyst. In **Chapter 3**, hence, CeO_2–ZrO_2–Bi_2O_3/SBA-16 was considered as a catalyst to remove organic compounds, and the catalytic removal performance for the refractory bisphenol-A was investigated.

List of Publications

1. Catalytic liquid-phase oxidation of acetaldehyde to acetic acid over a Pt/CeO_2-ZrO_2-SnO_2/γ-alumina catalyst

   Pilgyu Choi, Takanobu Ohno, Toshiyuki Masui, Nobuhito Imanaka

   Journal of Environmental Sciences, 2015, **36**, 63-66.

2. Catalytic liquid phase oxidation of 1,4-dioxane over a Pt/CeO_2-ZrO_2-Bi_2O_3/SBA-16 catalyst

   Pilgyu Choi, Takanobu Ohno, Nashito Fukuhara, Toshiyuki Masui, Nobuhito Imanaka

   Journal of Advanced Ceramics, 2015, **4**, 71-75.

3. High catalytic efficiency in liquid-phase oxidation of 1,4-dioxane using a Pt/CeO_2-ZrO_2-SnO_2/SBA-16 catalyst

   Pilgyu Choi, Naoyoshi Nunotani, Nobuhito Imanaka

   International Journal of Applied Ceramic Technology, in press.

4. Catalytic liquid-phase oxidation of bisphenol-A under moderate condition using CeO_2-ZrO_2-Bi_2O_3 supported on SBA-16

   Pilgyu Choi, Akito Kamijo, Naoyoshi Nunotani, Takeshi Nakano, Nobuhito Imanaka

   Chemistry Letters, in press.

Supplementary Publication

1. Catalytic liquid-phase oxidation of glycerol to dihydroxyacetone over a Pt/CeO_2-ZrO_2-Bi_2O_3/SBA-16 catalyst

   Pilgyu Choi, Naoyoshi Nunotani, Nobuhito Imanaka

   in preparation.

Chapter 1

Oxidation Removal of Hazardous Organic Compound Using catalyst in water

1.1. Introduction

As a material that can supply oxygen from inside the lattice, cerium–zirconium oxide (CeO_2–ZrO_2; CZ) is well known and used as promotor for purification of vehicle emission gas [26, 27]. This material can release the oxygen corresponding to the surrounding oxygen atmosphere, because cerium ion can take both tetravalent (Ce^{4+}) and trivalent (Ce^{3+}) state [28-30]. Moreover, by containing ZrO_2 into CeO_2, not only heat-resisting property but also the amount of oxygen up take and release from the material have increased [26, 27]. Furthermore, oxygen release and storage abilities are further increased by doping tin oxide (SnO_2) through an enhancement of redox property due to the valance charge of tin ion (Sn^{4+} and Sn^{2+}) [23, 31]. In water, therefore, facilitation of the oxidation owing to efficient supply of oxygen by using CeO_2–ZrO_2–SnO_2 (CZSn) is expected.

In chapter 1, acetaldehyde was selected as the hazardous organic compound to be removed by the catalysts. Acetaldehyde is widely used as a base material for synthetic resins, synthesis of acetic acid, and etc. However, it is identified as a cancer-causing substance [2, 32], so that effective removal of acetaldehyde from wastewater is required.

In order to remove acetaldehyde in water under moderate condition (under atmospheric pressure and below 100°C), I synthesized a catalyst by the combination of metallic Pt having a high catalytic

oxidation activity, CZSn exhibiting high oxygen release and storage abilities as a promotor, and γ-Al_2O_3 with high specific surface area as a support, and the catalytic performance of Pt/CZSn/γ-Al_2O_3 for acetaldehyde removal was investigated.

1.2. Experimental Procedure

Commercially available granular γ-Al_2O_3 (AxSorb AB, Axens) was ground in a mortar and mechanically pulverized for 2 h using a planetary ball-milling apparatus (Pulverisette7, FRITSCH GmbH). The fine γ-Al_2O_3 powder obtained was used for a catalyst support.

A CeO_2–ZrO_2–SnO_2(16 wt.%)/ γ-Al_2O_3 (CZSn/γ-Al_2O_3) composite was prepared by a co-precipitation process. The γ-Al_2O_3 support obtained above (2.11 g) was dispersed into a stoichiometric mixture of $Sn(C_2O_4)$ (0.0775 g) and aqueous solutions of 1.0 mol dm^{-3} $Ce(NO_3)_3$ (1.7 cm^3) and 0.1 mol dm^{-3} $ZrO(NO_3)_3$ (4.25 cm^3), where the molar ratio of Ce:Zr:Sn was controlled to be 68:17:15. Then, an aqueous solution of 3.0 mol dm^{-3} nitric acid was added into the fluid dispersion, and the mixture was stirred at room temperature for 30 min. The pH value was adjusted to 11 by the dropwise addition of aqueous ammonia. After stirring for 12 h at room temperature, the resulting precipitate was collected by filtration, washed several times with deionized water, and then dried at 80°C for 12 h. The dried powder was ground in a mortar and then calcined at 600°C for 1 h in an ambient atmosphere.

Finally, Pt was supported on the CZSn/γ-Al_2O_3 composite by impregnation of a platinum colloid stabilized with polyvinyl pyrrolidone (Tanaka Kikinzoku Kogyo Co., Ltd.). The amount of Pt on the catalyst was adjusted in a range from 5 to 10 wt.%. After impregnation, the solvent was evaporated at 180°C and the sample was dried at 80°C for 12 h. The dried powder was finally calcined at 500°C for 4 h in an ambient atmosphere. The obtained powders Pt (x wt.%; x = 5, 7, and

10)/$Ce_{0.68}Zr_{0.17}Sn_{0.15}O_{2.0}$ (16 wt.%)/γ-Al_2O_3 will hereafter denoted as Pt*x*/CZSn/γ-Al_2O_3.

The composition of the synthesized catalyst was analyzed with an X-ray fluorescence spectrometry (XRF, Supermini 200, Rigaku). The crystal structures of the synthesized catalysts were identified by X-ray powder diffraction (XRD, SmartLab, Rigaku) using Cu Kα radiation (40 kV, 30 mA) in the 2θ range from 10 to 70 degree. The Brunauer-Emmett-Teller (BET) specific surface area was measured at −196°C (Micromeritics Tristar 3000, Shimadzu) using N_2 adsorption.

The oxidation reaction of acetaldehyde in water was carried out under atmospheric pressure in bath mode using a mechanically stirred 300 cm^3 three-necked flask. An aqueous solution of 450 ppm acetaldehyde (10 cm^3) was poured into the flask and the catalyst (0.2 g) was loaded. The reactor was cooled in an ice bath at 0°C. After the reaction, catalyst was separated by centrifugation (Allegra 64R centrifuge, Beckman Coulter) and the supernatant liquid was analyzed using gas chromatograph-mass spectrometry (GC-MS, GCMS-QP2010 Plus, Shimadzu) to evaluate the acetaldehyde removal property and products. Removal percentage was calculated according to the equation (1):

$$\text{Removal percentage} = \frac{1-C_{\text{after}}}{1-C_{\text{before}}} \times 100\% \quad (1)$$

where C_{after} and C_{before} are the molar concentrations after and before the reaction, respectively.

1.3. Results and Discussion

The composition measured by XRF and BET surface area of the synthesized catalysts are summarized in Table 1.1. The compositions of the synthesized catalysts were confirmed to be in good agreement with the stoichiometric ratios of the starting materials within experimental error. The BET surface area of the γ-Al_2O_3 support was calculated to be 248 $m^2\ g^{-1}$ after the heat treatment at 600°C for 2 h. After the catalyst loading, the surface area decreased due to the result of the much larger density values of catalyst than those of the γ-Al_2O_3 support.

Table 1.1. Measured composition and BET surface area of the catalysts

Sample	Composition	BET surface area ($m^2\ g^{-1}$)
Pt5/CZSn/γ-Al_2O_3	Pt (5.4 wt.%)/$Ce_{0.66}Zr_{0.18}Sn_{0.16}O_{2.0}$ (16.6 wt.%)/γ-Al_2O_3	162
Pt7/CZSn/γ-Al_2O_3	Pt (6.4 wt.%)/$Ce_{0.64}Zr_{0.19}Sn_{0.19}O_{2.0}$ (15.9 wt.%)/γ-Al_2O_3	155
Pt10/CZSn/γ-Al_2O_3	Pt (9.3 wt.%)/$Ce_{0.65}Zr_{0.19}Sn_{0.19}O_{2.0}$ (15.2 wt.%)/γ-Al_2O_3	151

Figure 1.1 shows the XRD patterns of the Pt*x*/CZSn/γ-Al_2O_3 catalysts. The patterns contain diffraction peaks of metallic Pt, cubic fluorite-type of CZSn, and γ-Al_2O_3, and no crystalline impurities were observed. These results indicate that the objective catalysts were well synthesized.

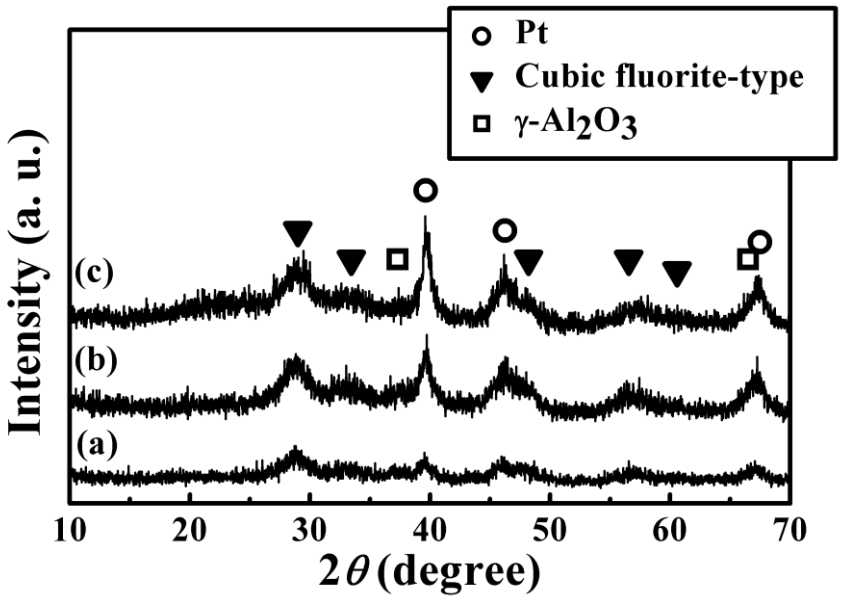

Figure 1.1. XRD patterns of the Pt*x*/CZSn/γ-Al_2O_3 catalysts; (a) $x = 5$, (b) $x = 7$, and (c) $x = 10$.

Figure 1.2 shows the dependences of the removal percentage for acetaldehyde on Pt content after the reaction under atmospheric pressure at 0°C. The removal property of all the catalysts was obviously recognized and high removal percentage of 70% or more were obtained without any supply of additives. Among the catalysts, Pt7/CZSn/γ-Al_2O_3 exhibited the highest removal property. It is estimated that the reason for the decrease of the removal percentage on Pt10/CZSn/γ-Al_2O_3 is the agglomeration and particle growth of the platinum particles [33] for the catalyst contented more than 7 wt.%. Accordingly, the optimum amount of Pt was approximately 7 wt.% in the present catalyst.

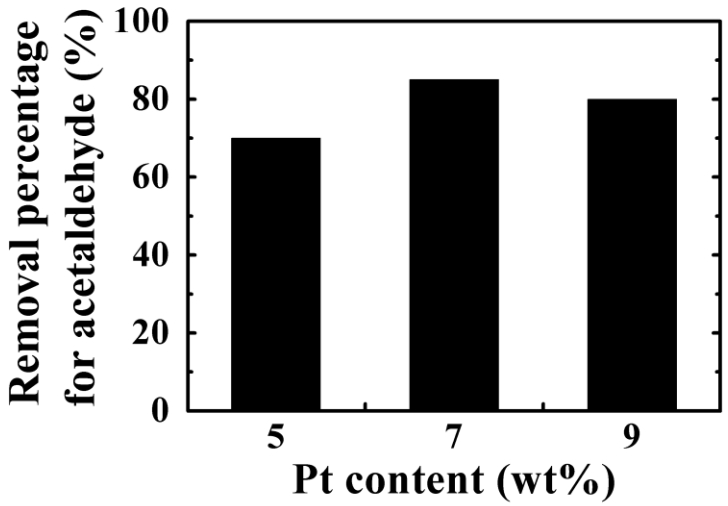

Figure 1.2. Pt content dependences of the removal percentage for acetaldehyde (1atm, 0°C).

For the Pt7/CZSn/γ-Al_2O_3 catalyst which exhibited the highest catalytic activity, the dependences of the removal percentage for acetaldehyde on the reaction time were investigated and the results are depicted in Figure 1.3. In the case of the absence of the catalyst, 5% of acetaldehyde was removed after the reaction for 8 h, due to the vaporization of highly volatile acetaldehyde. For the Pt7/CZSn/γ-Al_2O_3 catalyst, acetaldehyde in water was fully removed after the reaction for 8 h. Products after the reaction was investigated by using GC-MS. As a result, water, carbon dioxide, and acetic acid (91%) were detected, suggesting that acetaldehyde was oxidized to carbon dioxide through the acetic acid.

From these results, the Pt7/CZSn/γ-Al_2O_3 catalyst can remove 95% or more of acetaldehyde under atmospheric pressure atmosphere at 0°C for 8 h by oxidation reaction.

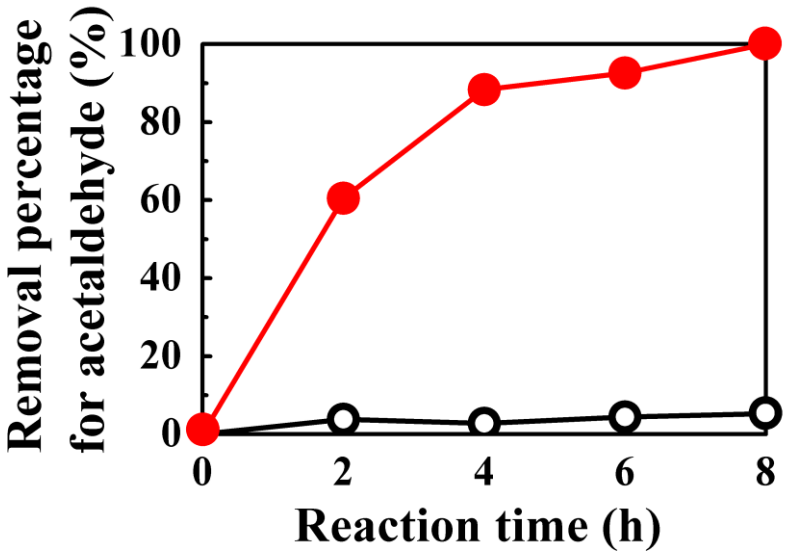

Figure 1.3. Reaction time dependences of the removal percentage for acetaldehyde on the Pt7/CZSn/γ-Al_2O_3 catalyst (1atm, 0°C); absence of the catalyst (○), presence of the catalyst (●).

1.4. Conclusions

In this chapter, the Pt*x*/CZSn/γ-Al_2O_3 catalysts were designed to efficiently remove acetaldehyde, which is one of the hazardous organic compound, in water under moderate condition. The catalysts were successfully synthesized by co-precipitation and impregnation processes. The synthesized catalysts exhibited high catalytic activity for acetaldehyde removal under atmospheric pressure at 0°C without any supply of additives. For the Pt7/CZSn/γ-Al_2O_3 catalyst, the highest catalytic activity was obtained due to the high dispersion of the catalyst, and acetaldehyde was fully removed in water by oxidation reaction after the reaction for 8 h.

Chapter 2

Enhancement of Catalytic Active Sites for Efficient Removal of Refractory Hazardous Organic Compound

2.1. Introduction

In the previous chapter, it was clear that the Pt/CZSn/γ-Al_2O_3 catalyst exhibited the high catalytic activity for acetaldehyde under moderate condition.

In this chapter, I focused on 1,4-dioxane which is more chemically stable as compared to acetaldehyde. 1,4-dioxane is a cyclic ether, and is an indispensable organic compound as a solvent in the chemical industry owing to its infinite solubility in water [34]; therefore, it has been widely used for the synthesis of many products. However, 1,4-dioxane has been identified as a cancer-causing pollutant [35], same as the acetaldehyde. Also, the distillation and centrifugation of 1,4-dioxane are difficult because of its similar boiling point (101°C) [34] and density (1.034 g cm^{-3}) [34] to those of water as well as its infinite solubility in water. Furthermore, 1,4-dioxane is refractory organic compound due to its chemically stable structure. Since the frequent use of 1,4-dioxane in chemical plants has led to the contamination of soil and water [36], regulations on emission standards regarding 1,4-dioxane are getting stricter [5]. For these reasons, 1,4-dioxane removal is important. However, its infinite solubility and non-biodegradable properties make it difficult to remove from wastewater. Thus, effective removal methods for 1,4-dioxane is required.

In the case of Pt/CZSn/γ-Al_2O_3, I have confirmed the low removal percentage (14%) for 1,4-

dioxane even at high reaction temperature of 80°C. Therefore, it is necessary to enhance the catalytic activity for efficient removal of 1,4-dioxane. In this chapter, I selected mesoporous silica SBA-16 (Santa Barbara Amorphous No. 16) as a support. Figure 2.1 shows the mesoporous structure of SBA-16. Since mesopores order regularly with a size of 12 nm interconnected via windows with a size of 5 nm [37, 38], SBA-16 possesses a high specific surface area of 787 m^2 g^{-1}, which is considerably higher than that of γ-Al_2O_3 (248 m^2 g^{-1}). Thereby, an enhancement of catalytic activity by an increase of catalytic active sites was expected.

From this concept, the Pt/CZSn supported on SBA-16 catalyst was synthesized and its catalytic removal performance for 1,4-dioxane was investigated. In addition, it is reported that CeO_2–ZrO_2–Bi_2O_3 also possessed high oxygen release and storage abilities [25]. Accordingly, the Pt/CeO_2–ZrO_2–Bi_2O_3/SBA-16 (Pt/CZBi/SBA-16) catalyst was also prepared, and the catalytic performance for 1,4-dioxane removal was investigated.

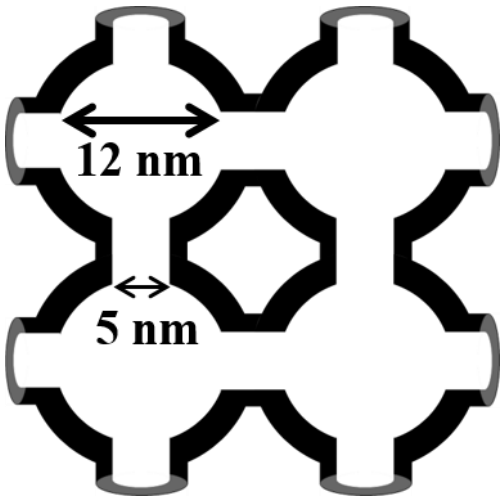

Figure 2.1. Mesoporous structure of SBA-16.

2.2. Experimental Procedure

SBA-16 was synthesized via a hydrothermal process according to the previous study [39]. Pluronic F-127 (1.6 g) and 1,3,5-trimethylbenzene (1.1 cm^3) were dissolved in 0.2 mol dm^{-3} hydrochloric acid (90 cm^3) and the solution was stirred at 35°C for 3 h. Then, tetraethyl orthosilicate (7.1 cm^3) was added and the solution was further stirred at 35°C for 20 h. The solution was poured into a Teflon bottle in a sealed brass vessel and heated at 140°C for 24 h. The product was collected by filtration and washed with deionized water and ethanol. The washed powder was dried at room temperature for 12 h and calcined at 400°C for 4 h in an air flow.

CeO_2–ZrO_2–SnO_2 (16 wt.%)/SBA-16 (CZSn/SBA-16) was synthesized using co-precipitation and impregnation processes. Aqueous solutions of 1.0 mol dm^{-3} $Ce(NO_3)_3$ (0.85 cm^3) and 0.1 mol dm^{-3} $ZrO(NO_3)_2$ (2.13 cm^3) were diluted with deionized water (50 cm^3), and $Sn(C_2O_4)$ (0.39 g) was added to the solution, where the molar ratio of Ce:Zr:Sn was controlled to be 68:17:15. The solution was stirred at room temperature until $Sn(C_2O_4)$ was dissolved. Then, synthesized SBA-16 (1.06 g) was dispersed into the solution, and this mixture was stirred at room temperature for 30 min. The pH value was adjusted to 11 by the dropwise addition of aqueous ammonia and the solution was stirred at room temperature for 12 h. The precipitated product was collected by filtration and washed with deionized water and ethanol. The powder was dried at 80°C for 12 h, and finally calcined at 900°C for 1 h in an ambient atmosphere.

CeO_2–ZrO_2–Bi_2O_3 (CZBi) was supported on the SBA-16 via an impregnation process. 1.0 mol dm^{-3} $Ce(NO_3)_3$ (0.30 cm^3), 0.1 mol dm^{-3} $ZrO(NO_3)_2$ (0.73 cm^3), and 0.5 mol dm^{-3} $Bi(NO_3)_3$ (0.13 cm^3) aqueous solutions were added to 50 cm^3 of deionized water, and the molar ratio of Ce:Zr:Bi was controlled in order to obtain a ratio of 68:17:15. Then, 0.4 g of synthesized SBA-16 was dispersed into the stoichiometric solution. The content of the CZBi solid solution was adjusted to be 16 wt.%. This mixture was stirred at room temperature for 6 h, and the solvent was vaporized at 180°C. The

obtained powder was ground in a mortar and calcined at 600°C for 1 h in an ambient atmosphere to obtain CeO_2–ZrO_2–Bi_2O_3 (16 wt.%)/SBA-16 (CZBi/SBA-16).

Pt was loaded on the CZSn/SBA-16 and CZBi/SBA-16 using a colloidal solution of Pt in ethanol stabilized with polyvinyl pyrrolidone (Tanaka Kikinzoku Kogyo K.K.). Here, the amount of Pt on the catalyst was adjusted to be 7 wt.%. After impregnation, the sample was dried at 80°C for 12 h, and calcined at 500°C for 4 h in an ambient atmosphere. The Pt/SBA-16 and Pt/CeO_2–ZrO_2/SBA-16 (Pt/CZ/SBA-16) catalysts were also synthesized for comparison. Here, the molar ratio of Ce:Zr was controlled to be 80:20.

The composition of the synthesized catalyst was analyzed with an X-ray fluorescence spectrometry (XRF, Supermini 200, Rigaku). The BET surface area and pore sized distribution were measured at −196°C using N_2 adsorption (Micromeritics Tristar 3000, Shimadzu). XRD (SmartLab, Rigaku) data were collected by a step scanning method in the 2θ range from 10 to 150 degree, using Cu Kα radiation (40 kV, 30 mA), and the XRD profiles were refined via the Rietveld method using RIETAN-FP program [40]. Small-angle X-ray scattering (SAXS, SmartLab, Rigaku) patterns were obtained in the 2θ range from 0.06 to 2.0 degree using Cu Kα radiation (40 kV, 30 mA). Transmission electron microscopy (TEM, H-800, Hitachi) was conducted to observe the morphology and size of the particles.

The oxidation reaction of 1,4-dioxane was conducted in a batch mode under atmospheric pressure. An aqueous solution of 100 ppm 1,4-dioxane (10 cm^3) was poured into the flask and the catalyst (0.3 g) was added into a 300 cm^3 three necked flask, and mechanically stirred. After reaction for 4 h at 40, 60, or 80°C, the catalyst and the solution were separated by centrifugation (Allegra 64R centrifuge, Beckman Coulter). The separated catalyst was dried at 80°C and reused for durability and reusability analysis. The solution was analyzed by GC-MS (GC-MS, GCMS-QP2010 Plus, Shimadzu) to determine the removal percentage for 1,4-dioxane. Mass spectra were recorded in the mass range from 15 to 150 amu in electronic impact mode. The temperature of the injector was set to 200°C and

the column (Rtx-624, Shimadzu) temperature program was set in the range from 50 to 100°C. Removal percentage was calculated according to the equation (1) in chapter 1. The reusability of the catalyst was examined by calculation using the equation (2):

$$\text{The reusability} = 1 - \frac{R_{\text{reused}}}{R_{\text{fresh}}} \quad (2)$$

where R_{fresh} and R_{reused} are removal percentages of 1,4-dioxane with fresh catalyst and reused catalyst, respectively. Temperature programmed reduction (TPR, Belcat-B, MicrotracBEL) measurement was carried out under a flow of 5% H_2/Ar (50 cm^3 min^{-1}) at a heating rate of 5°C min^{-1} in the temperature range from 50 to 400°C.

2.3. Results and Discussion

2.3.1. Pt/CeO_2–ZrO_2–SnO_2/SBA-16 catalyst

The composition of the synthesized catalyst was confirmed to be in good agreement with the stoichiometric ratio of the starting materials (Pt (7 wt.%)/$Ce_{0.68}Zr_{0.17}Sn_{0.15}O_2$ (16 wt.%)/SBA-16; Pt/CZSn/SBA-16) within experimental error by XRF.

Figure 2.2 shows the N_2 adsorption-desorption isotherms of synthesized Pt/CZSn/SBA-16, Pt/SBA-16, and SBA-16. According to the Brunauer–Deming–Deming–Teller (BDDT) classification, the isotherm of SBA-16 is classified as type IV, which can be observed in materials with mesoporous structure. Also, it shows a hysteresis loop of type H2, according to the International Union of Pure and Applied Chemistry (IUPAC), indicating that the material consists of pores which are regular size and interconnected via small windows [37, 38]. The BET specific surface area was calculated to be 787 m^2 g^{-1}. From these results, SBA-16 possesses the high surface area due to the mesoporous structure. After the Pt and Pt/CZSn catalysts loading, the isotherms maintained the equivalent classification to SBA-16, indicating that the mesoporous structure of SBA-16 was preserved and the

mesopores were still interconnected. BET specific surface areas of Pt/SBA-16 and Pt/CZSn/SBA-16 were calculated to be 579 m^2 g^{-1} and 273 m^2 g^{-1}, respectively. The decreases of surface areas after catalysts loading suggest that the catalysts were inserted into the mesopores of SBA-16. Here, the surface area of Pt/CZSn/SBA-16 (273 m^2 g^{-1}) was increased as compared to that of Pt7/CZSn/γ-Al_2O_3 (155 m^2 g^{-1}) by using SBA-16 as a support.

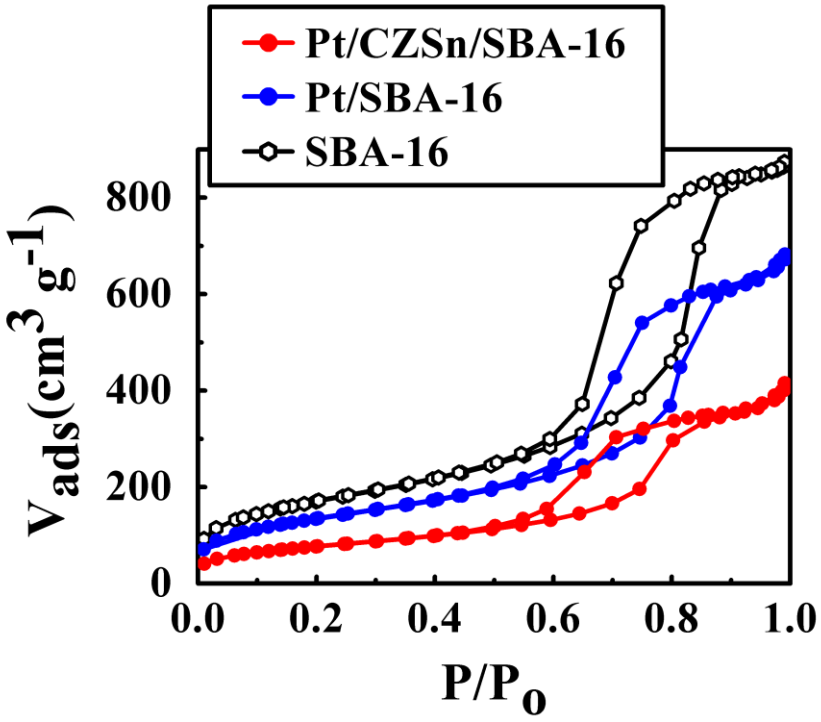

Figure 2.2. N_2 adsorption-desorption isotherms of Pt/CZSn/SBA-16, Pt/SBA-16, and SBA-16.

The pore size distribution profiles were calculated from the N_2 adsorption-desorption isotherms using the Barrett–Joyner–Halenda (BJH) analysis, and the results are depicted in the Figure 2.3. For SBA-16, two peaks were observed (marked as filled inverted triangle) at ca. 5 nm and ca. 12 nm. The N_2 adsorption-desorption isotherms and this pore size distribution indicate that mesopores with a size of ca. 12 nm were interconnected via windows with a size of ca. 5 nm. For the Pt/SBA-16 and Pt/CZSn/SBA-16 catalysts, decreases of pore diameter and pore volume were observed relative to SBA-16, suggesting that the mesopores were filled with the catalysts.

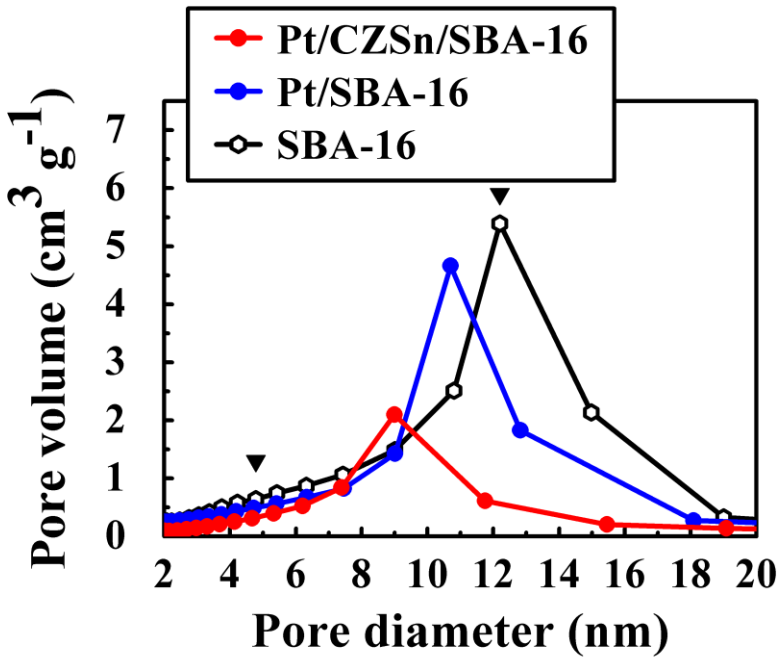

Figure 2.3. Pore size distribution profiles of Pt/CZSn/SBA-16, Pt/SBA-16, and SBA-16.

Figure 2.4 shows the results of the Rietveld refinement for the XRD pattern of Pt/CZSn/SBA-16 and Pt/CZ/SBA-16. For the Rietveld analysis, I used the pattern of the SBA-16 support as a background and the occupations of each cation were the results estimated from the XRF. From the Rietveld analysis for Pt/CZSn/SBA-16, all the diffraction peaks were indexed as a cubic fluorite-type structure of CZSn (green line) and Pt (pink line), and no impurity phases were observed. For Pt/CZ/SBA-16, the diffraction peaks were indexed as only a cubic fluorite-type structure and Pt.

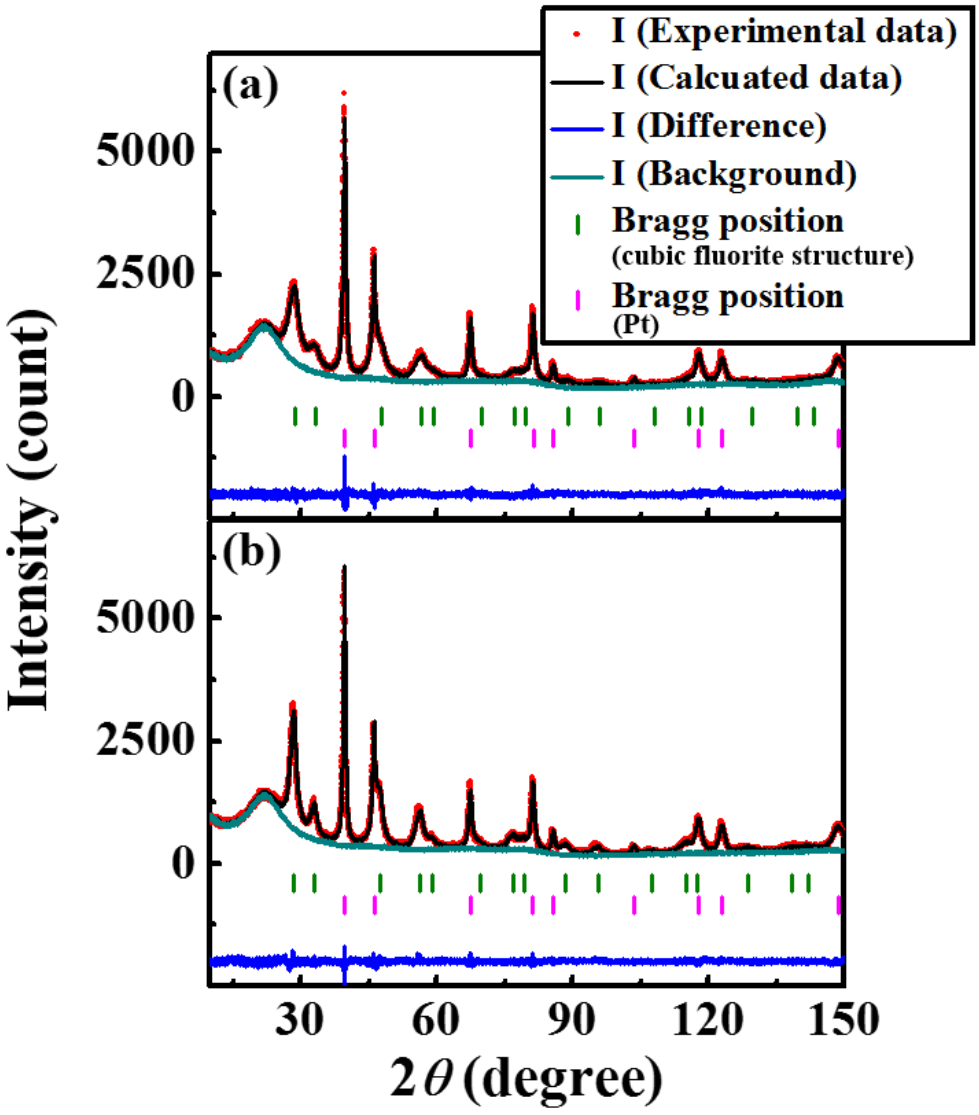

Figure 2.4. Results of the Rietveld analysis for (a) Pt/CZSn/SBA-16 and (b) Pt/CZ/SBA-16.

The structural parameters of cubic fluorite-type phase are summarized in Table 2.1. A lattice shrinkage for the fluorite-type structure (CZSn: 0.5383 nm, CZ: 0.5403 nm) was observed by introducing Sn ions, because the average cationic radius of the 4*a* site in the CZSn (0.092 nm) is smaller than that of the CZ (0.095 nm). Here, the average cationic radii were calculated from the occupations and ionic radii of each cation: 0.097 nm for Ce, 0.084 nm for Zr, and 0.081 nm for Sn (coordination number = 8) [41]. From the result of oxygen occupation for CZ (0.955), the formation of oxygen vacancies was confirmed, and it is due to the partial reduction of Ce^{4+} to Ce^{3+} [30]. By introducing Sn ions into the CZ lattice, the oxygen occupation (0.919) decreased as comparison to that of CZ, due to the partial reduction of Sn^{4+} to Sn^{2+} [31].

Table 2.1. Structural parameters of cubic fluorite-type phase for the Pt/CZSn/SBA-16 and Pt/CZ/SBA-16

Sample	Lattice Parameter (nm)	Atom	Wyckoff Position	Occupation	*x*	*y*	*z*	*B*(Å^2)
Pt/CZSn/SBA-16	0.5383(1)	Ce	4*a*	0.69	0	0	0	1
		Zr	4*a*	0.16	0	0	0	1
		Sn	4*a*	0.15	0	0	0	1
		O	8*c*	0.919(11)	1/4	1/4	1/4	1
Space group: $Fm\bar{3}m$, R_{wp} = 5.52%, S = 1.38								
Pt/CZ/SBA-16	0.5403(1)	Ce	4*a*	0.80	0	0	0	1
		Zr	4*a*	0.20	0	0	0	1
		O	8*c*	0.955(9)	1/4	1/4	1/4	1
Space group: $Fm\bar{3}m$, R_{wp} = 5.46%, S = 1.35								

To confirm the regular arrangement of the mesopores of SBA-16, the diffraction patterns at small angles were investigated. Figure 2.5 shows the SAXS patterns of Pt/CZSn/SBA-16, Pt/SBA-16, and SBA-16. For SBA-16, since diffraction peaks assigned to the (110) and (200) plane [37, 38] were clearly observed at 0.56 and 1.10 degree, respectively, SBA-16 possesses arranged mesopores with a regular pore diameter. After loading the Pt and Pt/CZSn catalysts, the peak intensities were decreased, caused by a slight loss of periodicity in the mesopores of SBA-16. In addition, the peaks shifted to higher angles, suggesting that pore diameter of SBA-16 was decreased. These results also indicate that the catalysts were loaded into the mesopores of SBA-16.

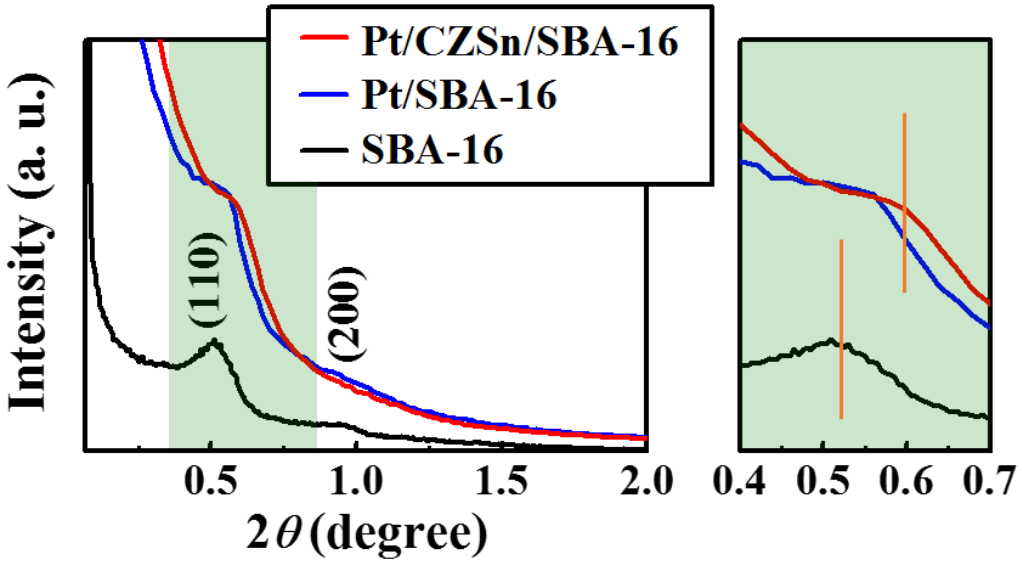

Figure 2.5. SAXS patterns of Pt/CZSn/SBA-16, Pt/SBA-16, and SBA-16.

Another evidence for the insertion of the catalysts into the mesopores of SBA-16 was provided by TEM observation. TEM and electron diffraction images of Pt/CZSn/SBA-16 are shown in Figure 2.6. The Pt/CZSn/SBA-16 catalyst possessed a regular arrangement of pores with a diameter of ca. 12 nm. Pt particles were observed as dark spots in and/or on the mesopores of SBA-16. Although it is difficult to distinguish between CZSn and SBA-16 on the TEM image, the electron diffraction image was clearly indexed to the same positions as the cubic fluorite-type structure of CZSn. These results demonstrate that Pt and CZSn were well dispersed into the mesopores of SBA-16 and show good agreement with the results of N_2 adsorption-desorption isotherms, pore size distribution, XRD, and SAXS, described above.

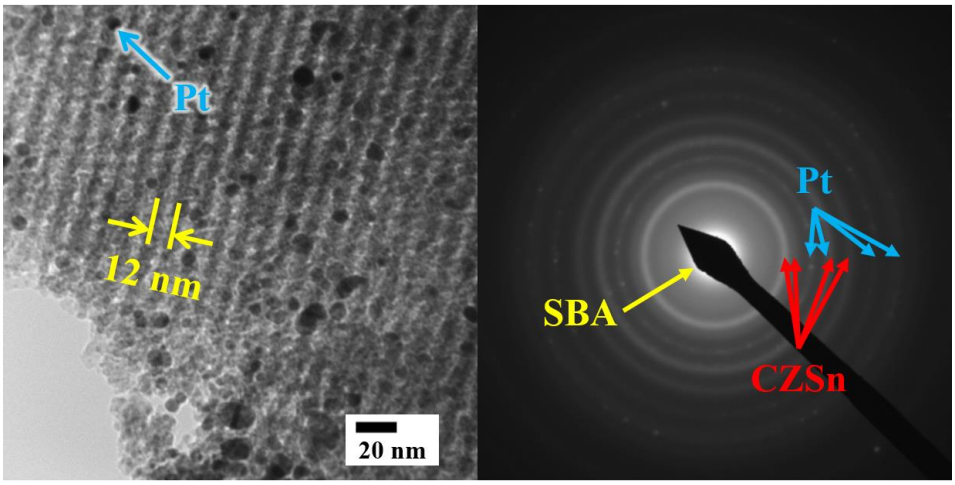

Figure 2.6. TEM and electron diffraction images of Pt/CZSn/SBA-16.

Figure 2.7 shows reaction temperature dependences of the removal percentage for 1,4-dioxane on the Pt/CZSn/SBA-16, Pt/SBA-16, and SBA-16 under atmospheric pressure for 4 h. Although the SBA-16 support showed the removal performance of 1,4-dioxane, the removal percentage was almost constant, i.e., independent with reaction temperature, which is due to vaporization and adsorption on and in the mesoporous structure of SBA-16 with a large surface area (787 m^2 g^{-1}). On the other hand, in the cases of Pt/SBA-16 and Pt/CZSn/SBA-16, the removal percentages increased with an increase in reaction temperature, so that these catalysts processed the oxidation activity. The highest catalytic activity was obtained for the Pt/CZSn/SBA-16 catalyst owing to the promotion of oxygen supply to the Pt from the CZSn lattice, and a removal percentage was achieved to 69% after the reaction at 80°C.

Products after the reaction was investigated by using GC-MS. For SBA-16, only water and 1,4-dioxane were detected without any products. Whereas, in the case of the Pt/CZSn/SBA-16 catalyst, carbon dioxide was detected in addition to water and 1,4-dioxne, indicating that oxidation reaction successfully occurred. Furthermore, since no other compound was detected, it is clear that 1,4-dioxane oxidation to harmless carbon dioxide and water was completely proceeded by catalytic decomposition process.

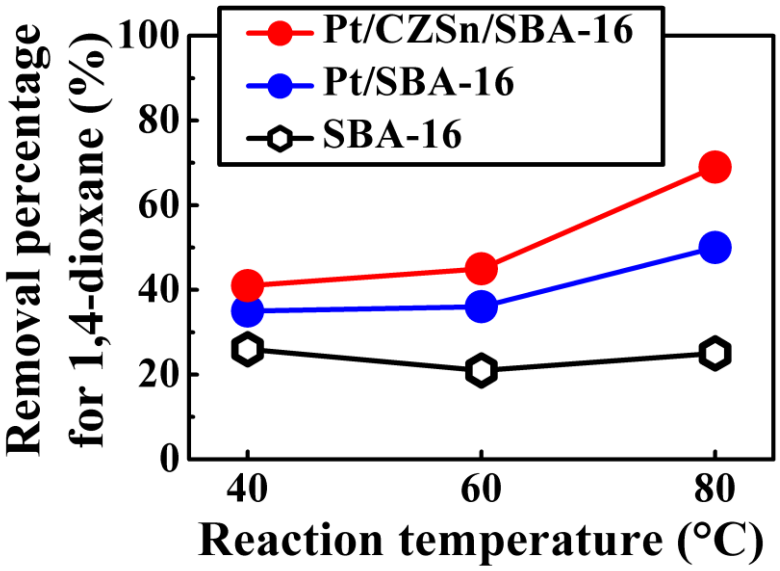

Figure 2.7. Reaction temperature dependences of the removal percentage for 1,4-dioxane on the Pt/CZSn/SBA-16, Pt/SBA-16, and SBA-16 (1atm, 4 h).

To examine reusability, the catalyst was reused for the catalytic oxidation of 1,4-dioxane without being washed. The reusabilities were identified by the R_{reused}/R_{fresh} ratio (R_{fresh} : removal percentage with fresh catalyst, R_{reused} : removal percentages with reused catalyst), and the results are shown in Figure 2.8. For SBA-16, the catalytic activities after consecutive usage were obviously decreased, because the 1,4-dioxane adsorbed in the first cycle impeded further adsorption. On the other hand, in the case of Pt/CZSn/SBA-16 catalyst, the catalytic activities were almost maintained with high values over 90%, because almost of 1,4-dioxane was removed by the oxidation reaction. These results indicate that the Pt/CZSn/SBA-16 catalyst possessed the high reusability and the catalytic oxidation reaction proceeded continuously.

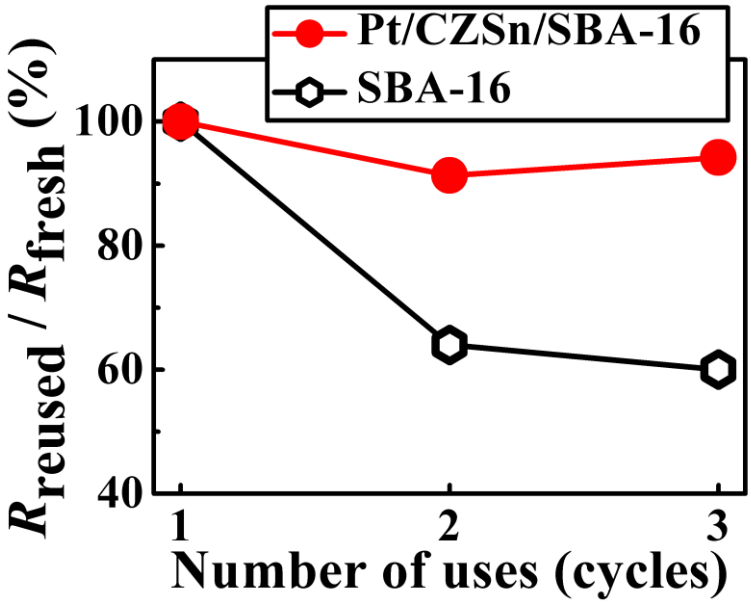

Figure 2.8. Reaction cycle dependences of the removal percentage for 1,4-dioxane on the Pt/CZSn/SBA-16, and SBA-16 (1atm, 4 h, 80°C).

2.3.2. Pt/CeO_2–ZrO_2–Bi_2O_3/SBA-16 catalyst

The composition of the synthesized catalyst was confirmed to be in good agreement with the stoichiometric ratio of the starting materials (Pt (7 wt.%)/$Ce_{0.68}Zr_{0.17}Bi_{0.15}O_2$ (16 wt.%)/SBA-16) within experimental error by XRF.

Figure 2.9 shows the N_2 adsorption-desorption isotherms of Pt/CZBi/SBA-16 and SBA-16. For the Pt/CZBi/SBA-16 catalyst, the isotherms maintained the equivalent classification to SBA-16, indicating that the mesoporous structure of SBA-16 was preserved and the mesopores were still interconnected. The BET specific surface area of Pt/CZBi/SBA-16 was calculated to be 475 $m^2\ g^{-1}$. A decrease of the BET specific surface area after catalysts loading was also observed as compared to SBA-16 (787 $m^2\ g^{-1}$), suggesting that Pt and CZBi were inserted into the mesopores of SBA-16.

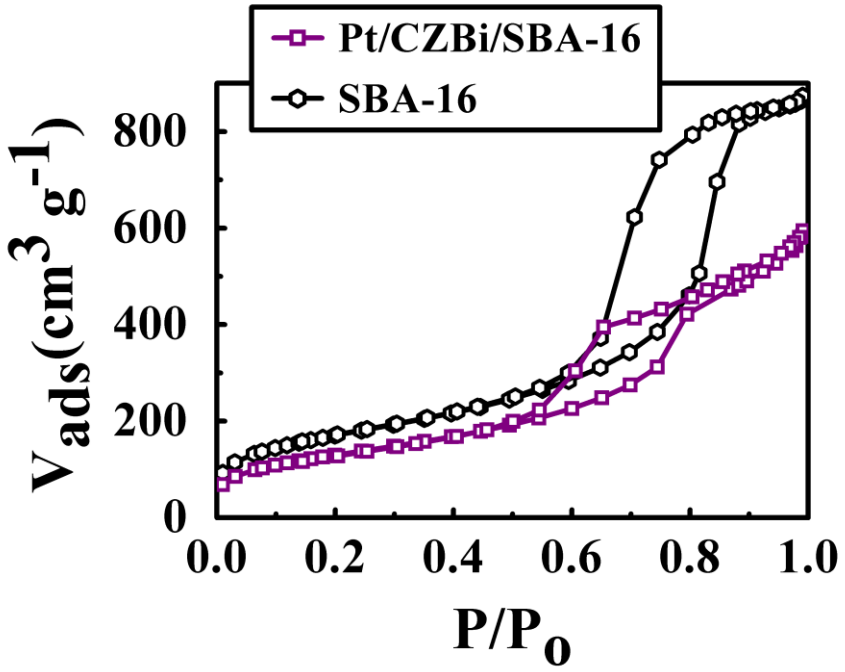

Figure 2.9. N_2 adsorption-desorption isotherms of Pt/CZBi/SBA-16 and SBA-16.

The pore size distribution profile of Pt/CZBi/SBA-16 was calculated from the N_2 adsorption-desorption isotherm using the BJH analysis, and the result is depicted in Figure 2.10 for comparison with the data for SBA-16. For the Pt/CZBi/SBA-16 catalyst, pore diameter and pore volume were decreased compared to SBA-16, suggesting that the mesopores were filled with the catalysts.

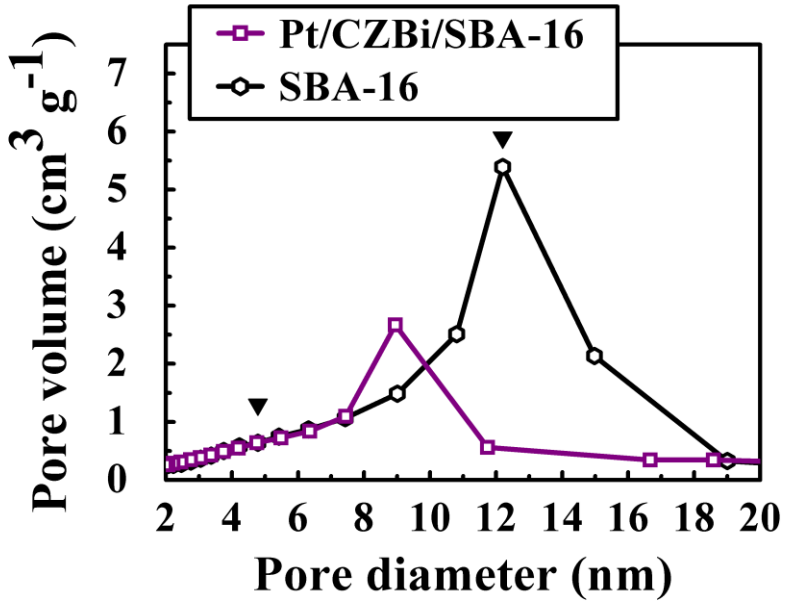

Figure 2.10. Pore size distribution profiles of Pt/CZBi/SBA-16 and SBA-16.

Figure 2.11 shows the result of the Rietveld refinement for the XRD pattern of Pt/CZBi/SBA-16. For the Rietveld analysis, I used the pattern of the SBA-16 support as a background and the occupations of each cation were the results estimated from the XRF. From the Rietveld analysis for Pt/CZBi/SBA-16, all the diffraction peaks were indexed as a cubic fluorite-type structure of CZBi (green line) and Pt (pink line), and no impurity phases were observed.

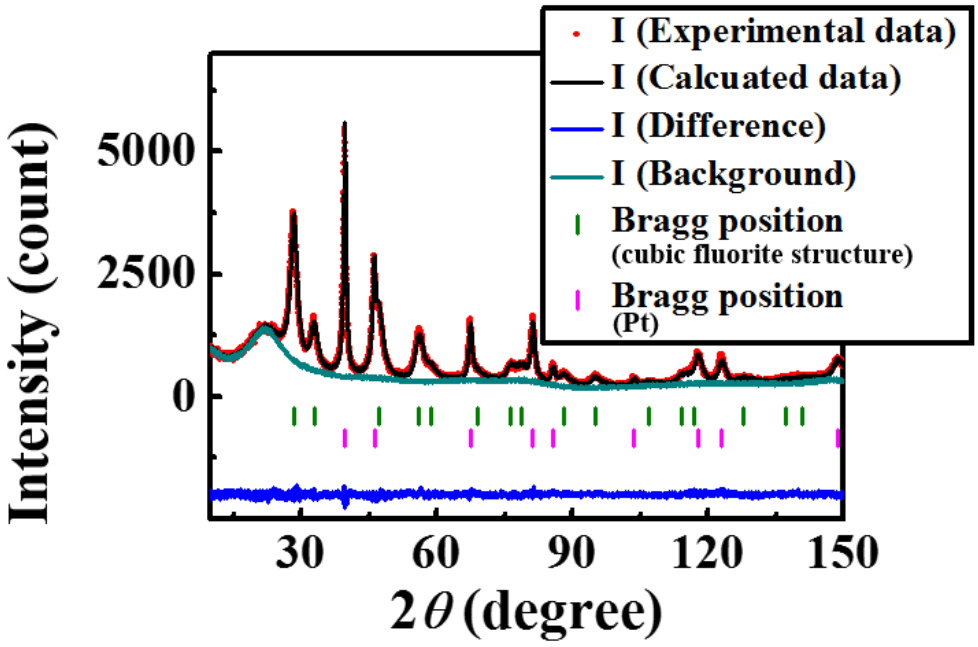

Figure 2.11. Result of the Rietveld analysis for Pt/CZBi/SBA-16.

The structural parameters of cubic fluorite-type phase are summarized in Table 2.2 for the comparison with the data for Pt/CZ/SBA-16. A lattice expansion of the fluorite-type structure (CZBi: 0.5426 nm, CZ: 0.5403 nm) was observed by introducing Bi ions, because the average cationic radius at the 4*a* site in the CZBi (0.098 nm) is larger than that of the CZ (0.095 nm). Here, the average cationic radii were calculated from the occupations and ionic radii of each cation: 0.097 nm for Ce, 0.084 nm for Zr, and 0.117 nm for Bi (coordination number = 8) [41]. By introducing Bi ions into the CZ lattice, the oxygen occupation (0.847) decreased as comparison to those of CZ (0.955) and CZSn (0.919), due to lower-valent of Bi^{3+} ions, indicating that an additional oxygen vacancy was formed.

Table 2.2. Structural parameters of cubic fluorite-type phase for the Pt/CZBi/SBA-16 and Pt/CZ/SBA-16

Sample	Lattice Parameter (nm)	Atom	Wyckoff Position	Occupation	*x*	*y*	*z*	*B*(Å^2)
Pt/CZBi/SBA-16	0.5426(1)	Ce	4*a*	0.69	0	0	0	1
		Zr	4*a*	0.16	0	0	0	1
		Sn	4*a*	0.15	0	0	0	1
		O	8*c*	0.847(7)	1/4	1/4	1/4	1
Space group: $Fm\bar{3}m$, R_{wp} = 5.20%, S = 1.35								
Pt/CZ/SBA-16	0.5403(1)	Ce	4*a*	0.80	0	0	0	1
		Zr	4*a*	0.20	0	0	0	1
		O	8*c*	0.955(9)	1/4	1/4	1/4	1
Space group: $Fm\bar{3}m$, R_{wp} = 5.46%, S = 1.35								

Figure 2.12 shows the SAXS patterns of Pt/CZBi/SBA-16 and SBA-16. In the case of the Pt/CZBi/SBA-16 catalyst, the peak intensities of (110) and (200) [37, 38] were decreased due to a slight loss of periodicity of the mesopores in SBA-16. In addition, the peaks shifted to higher angles, indicating the decrease of pore diameter of SBA-16. These results also suggest that Pt and CZBi were loaded into the mesopores of SBA-16.

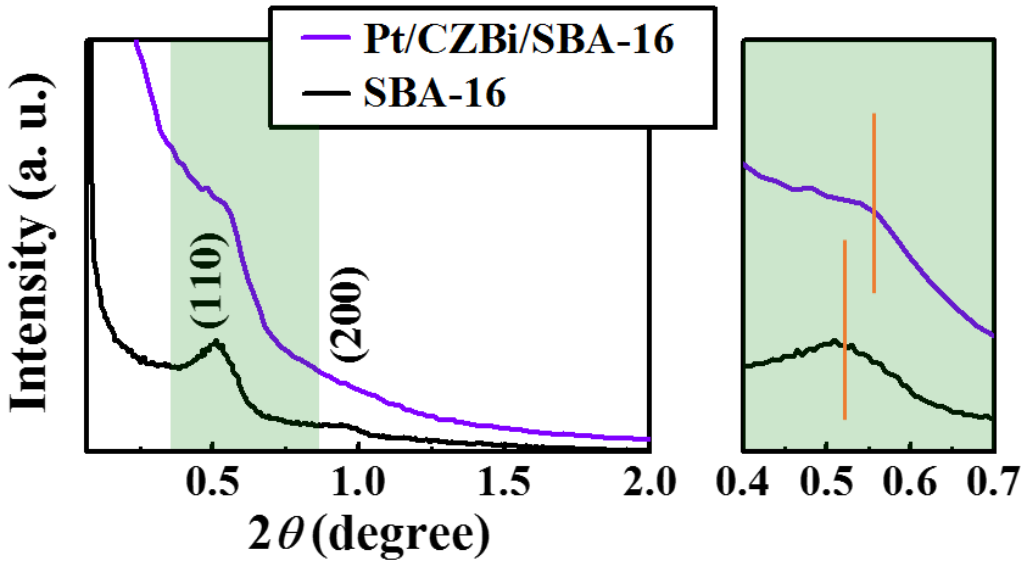

Figure 2.12. SAXS patterns of Pt/CZBi/SBA-16 and SBA-16.

TEM and electron diffraction images of Pt/CZBi/SBA-16 are shown in Figure 2.13. The Pt/CZBi/SBA-16 catalyst possessed a regular arrangement of pores with a diameter of ca. 12 nm. Pt particles were observed as dark spots in and/or on the mesopores of SBA-16. Although it is difficult to distinguish between CZBi and SBA-16 on the TEM image, the electron diffraction image was clearly indexed to the same positions as cubic fluorite-type structure of CZBi. These results demonstrate that Pt and CZBi were well dispersed into the mesopores of SBA-16 and show good agreement with the results of N_2 adsorption-desorption isotherms, pore size distribution, XRD, and SAXS, described above.

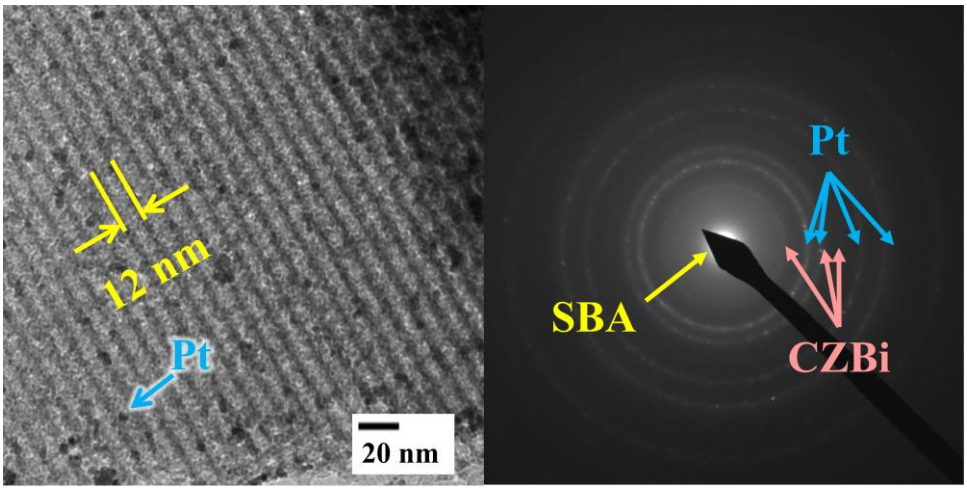

Figure 2.13. TEM and electron diffraction images of Pt/CZBi/SBA-16.

Figure 2.14 shows reaction temperature dependences of the removal percentage for 1,4-dioxane on the Pt/CZBi/SBA-16 under atmospheric pressure for 4 h. For comparison, results in the cases of SBA-16, Pt/SBA-16, and Pt/CZSn/SBA-16 are also depicted. For Pt/CZBi/SBA-16, since the removal percentage increased with an increase in the reaction temperature, the catalytic process was assumed to have proceeded successfully. In addition, the removal percentages for Pt/CZBi/SBA-16 were higher than those for Pt/SBA, indicating that catalytic activity was promoted by introducing CZBi owing to high oxygen release and storage abilities. After the reaction at 80°C, the removal percentage reached up to 59%. However, it is lower than that in the case for Pt/CZSn/SBA-16 (69%).

Products after the reaction using Pt/CZBi/SBA-16 was investigated by using GC-MS. As a result, only carbon dioxide, water, and 1,4-dioxane were detected, indicating that oxidation reaction proceeded completely.

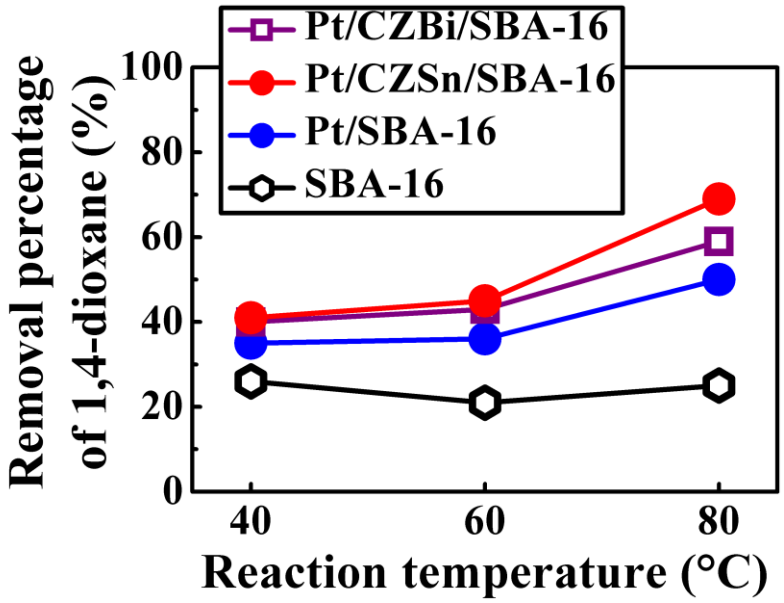

Figure 2.14. Reaction temperature dependences of the removal percentage for 1,4-dioxane on the Pt/CZBi/SBA-16, SBA-16, Pt/CZB-16 and Pt/CZSn/SBA-16 (1atm, 4 h).

2.3.3. Oxygen release property of the catalysts

To investigate the reason for the higher catalytic activity of Pt/CZSn/SBA-16 as compared to that of Pt/CZBi/SBA-16, TPR analysis was carried out, and results are shown in Figure 2.15 with the result of Pt/CZ/SBA-16. For Pt/CZ/SBA-16, the reduction was observed in the temperature range from 200°C to 350°C, which attributed to the reduction of Ce^{4+} to Ce^{3+}, and the reduction split to two separate peaks due to accelerated reduction by the oxygen spillover from the CZ to Pt [24, 42]. For Pt/CZBi/SBA-16, the reduction of Ce^{4+} to Ce^{3+} was observed in the temperature range from 200°C to 350°C, and significant enhancement of the reducibility was due to the formation of oxide ion vacancies by introducing lower-valent of Bi^{3+} ions, leading the enhancement of the mobility of lattice oxygen to the catalyst [25]. For Pt/CZSn/SBA-16, reduction peaks attributed to reduction of Ce^{4+} to Ce^{3+} in the temperature range from 200°C to 350°C was also observed. Furthermore, additional reduction was observed peak at ca. 100°C, because it is likely that the reduction of Sn^{4+} to Sn^{2+} was accelerated by the electron transfer between Pt and Sn [43, 44]. Therefore, Pt/CZSn/SBA-16 showed the higher activity owing to easily reduction at low temperature as compared to Pt/CZBi/SBA-16. Consequently, the highest catalytic removal performance was obtained for Pt/CZSn/SBA-16 by synergistic effects between the CZSn promoter and the Pt catalyst with high dispersion.

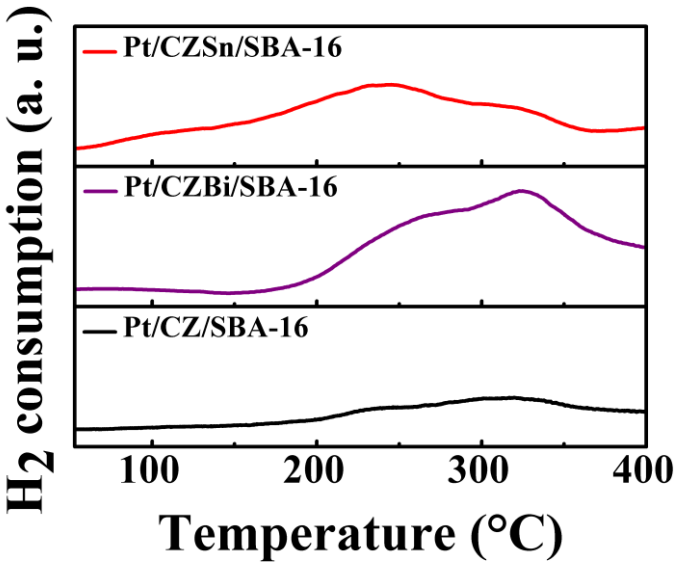

Figure 2.15. TPR profiles of Pt/CZSn/SBA-16, Pt/CZBi/SBA-16, and Pt/CZ/SBA-16.

2.4. Conclusions

In this chapter, for efficient removal of 1,4-dioxane, which is one of the refractory hazardous organic compound in water, under moderate condition, I tried to increase the catalytic active sites by selecting SBA-16 with the considerably high surface area as a support.

The Pt/CZSn and Pt/CZBi were successfully dispersed in and/or on the regularly arranged mesopores of SBA-16 by impregnation and co-precipitation processes. The novel Pt/CZSn/SBA-16 and Pt/CZBi/SBA-16 catalysts possessed high surface areas and exhibited high catalytic activities under atmospheric pressure at 80°C for 1,4-dioxane removal. Removal percentages were reached up to 69% and 59% after the reaction for 4 h on Pt/CZSn/SBA-16 and Pt/CZBi/SBA-16, respectively. Furthermore, the oxidation of 1,4-dioxane proceeded completely to harmless carbon dioxide and water without byproducts. The highest catalytic activity was obtained for the combination of Pt, CZSn, and SBA-16 by synergistic effect between the high oxygen release and storage abilities of CZSn and the high reactivity of Pt with high dispersion. Additionally, the Pt/CZSn/SBA-16 catalyst possessed the high reusability.

Chapter 3

Oxidation Removal of Refractory Hazardous Organic Compound Using Precious Metal-free Catalyst

3.1. Introduction

Bisphenol-A (BPA), a refractory hazardous compound, is widely used in chemical industry as an intermediate in the manufacturing of epoxy resins and polycarbonate plastics in food and beverage containers [3, 4]. However, it has been identified as an endocrine-disrupting chemical with an estrogenic function in living organism even at very low concentrations [3, 4]. Thus, even a small amount of BPA from food and beverage containers dissolving into the soil and water supply would negatively affect the environment and human health. In addition, BPA also possesses non-biodegradable property. Therefore, to protect the environment and our health, effective removal methods for BPA is required. Although a recent report found that BPA removal was proceeded by Ag/CZ under the high pressure (20 atm) and the high temperature (160°C) [22], the moderate condition (under air atmosphere below 100°C) is required for practical use.

In the previous chapter, the high catalytic activities were realized on Pt/CZSn/SBA-16 and Pt/CZBi/SBA-16, due to the oxidative activity of Pt, the high oxygen release and storage abilities of promoters, and the high surface area of SBA-16. In this chapter, I expected that the materials using only CZM (M = Sn, Bi) promoter and SBA-16 also work as a catalyst. A comparison of CZSn/SBA-16 and CZBi/SBA-16 reveals that CZBi/SBA-16 exhibited the higher oxygen release ability, as

shown in Figure 3.1. Accordingly, catalytic removal performance of BPA was investigated for the CZBi/SBA-16 catalyst.

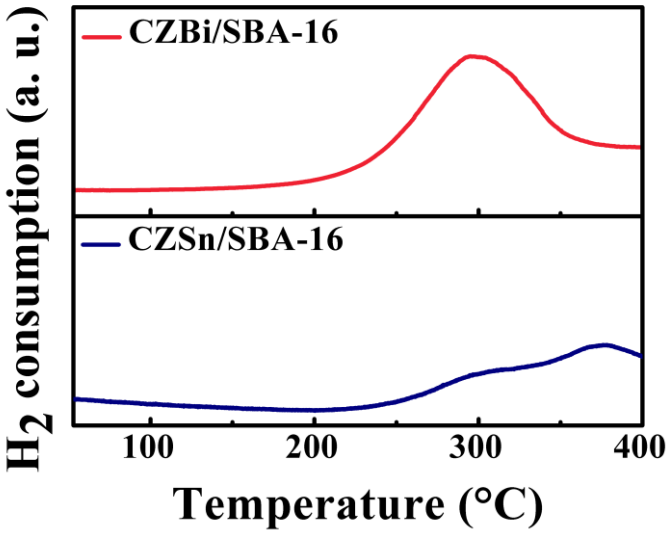

Figure 3.1. TPR profiles of CZBi/SBA-16 and CZSn/SBA-16.

3.2. Experimental Procedure

The CZBi/SBA-16 catalyst was prepared by the similar procedure described in Chapter 2. For comparison, a CZ supported on SBA-16 was also synthesized. Here, the molar ratio of Ce:Zr was controlled to be 85:15, and the contents of the CZ solid solution was adjusted to be 16 wt.%.

XRD (MultiFlex, Rigaku) data were collected by a step scanning method in the 2θ range from 10 to 150 degree using Cu Kα radiation (40 kV, 40 mA), and the XRD profiles were refined via the Rietveld method using RIETAN-FP program [40]. Also, the XRF (Supermini 200, Rigaku), BET (Micromeritics Tristar 3000, Shimadzu), SAXS (SmartLab, Rigaku), TEM (H-800, Hitachi), and TPR measurement (Belcat-B, MicrotracBEL) on identical conditions in chapter 2 were carried out to characterize properties of the catalyst.

The oxidation reaction of BPA was conducted in an air atmosphere in batch mode using a mechanically stirred 300 cm^3 three necked flask. An aqueous solution of 50 ppm BPA (10 cm^3) was poured into the flask and the catalyst (0.3 g) was added. After reaction for 3 h at 80°C, the catalyst and the solution were separated by centrifugation (Allegra 64R centrifuge, Beckman Coulter). The separated catalyst was dried at 80°C and reused for durability and reusability analysis. The solution (2 cm^3) was mixed with dichloromethane (2 cm^3) to extract BPA. The BPA extracted with dichloromethane was analyzed by GC-MS (Bruker, 450-GC and 320-MS) to determine the removal percentage for BPA. Mass spectra were recorded in the mass range from 50 to 500 amu on TQ mass spectrometer that was operating in the electronic impact mode. The temperature of the injector was set at 300°C, and the temperature program of the column (Varian, CP8142) was set in the range from 120 to 300°C. Removal percentage was calculated according to the equation (1) in chapter 1. The reusability of the catalyst was examined by calculation using the equation (2) in chapter 2.

3.3. Results and Discussion

The composition of the synthesized catalyst was confirmed by XRF to be in good agreement with the stoichiometric ratio of the starting materials ($Ce_{0.68}Zr_{0.17}Bi_{0.15}O_{1.925}$ (16 wt.%)/SBA-16) within experimental error. Figure 3.2 shows the N_2 adsorption-desorption isotherms of synthesized CZBi/SBA-16, CZ/SBA-16, and SBA-16. After loading CZ and CZBi, the isotherms retained the equivalent classification to SBA-16, indicating that the mesoporous structure of SBA-16 was preserved and the mesopores were still interconnected. BET specific surface areas of CZ/SBA-16 and CZBi/SBA-16 were calculated to be 561 $m^2\ g^{-1}$ and 502 $m^2\ g^{-1}$, respectively. The decrease of the surface area after loading CZ or CZBi on SBA-16 (787 $m^2\ g^{-1}$) was observed, suggesting that the CZ or CZBi were inserted into the mesopores of SBA-16. As compared with an unsupported CZBi (46 $m^2\ g^{-1}$) [45], CZBi/SBA-16 possessed the considerably increased surface area.

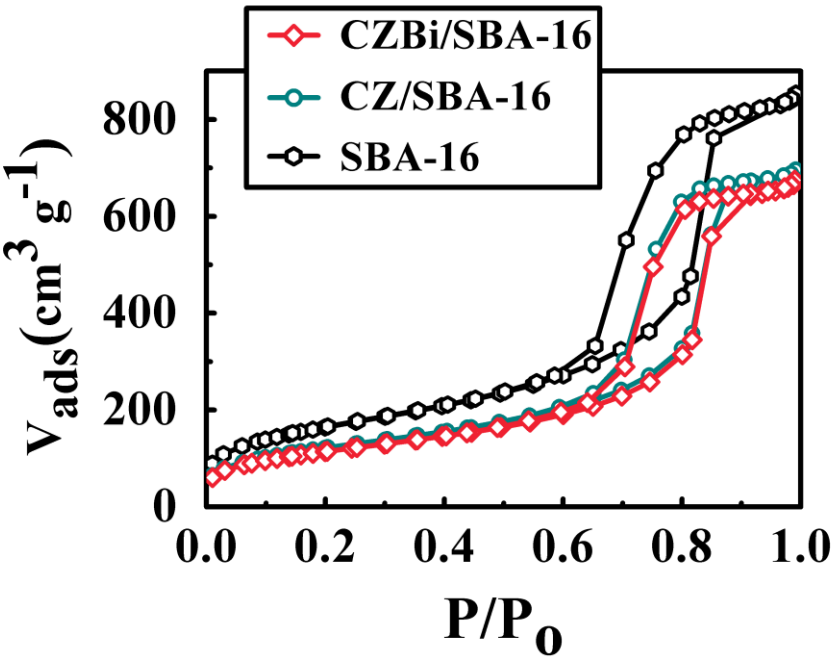

Figure 3.2. N_2 adsorption-desorption isotherms of CZBi/SBA-16, CZ/SBA-16, and SBA-16.

The pore size distribution profiles were calculated from the N_2 adsorption-desorption isotherms of CZBi/SBA-16, CZ/SBA-16, and SBA-16 using the BJH analysis, and the results are depicted in the Figure 3.3. For the CZ/SBA-16 and CZBi/SBA-16 catalyst, slight decreases of pore volume were observed, suggesting that the mesopore were filled with the catalysts.

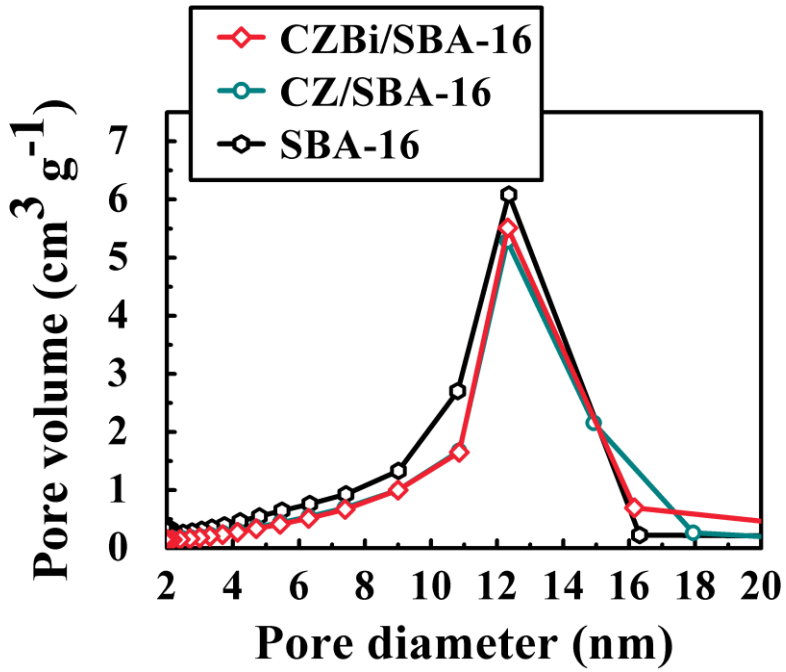

Figure 3.3. Pore size distribution profiles of CZBi/SBA-16, CZ/SBA-16, and SBA-16.

Figure 3.4 shows the SAXS patterns of CZBi/SBA-16, CZ/SBA-16 and SBA-16. In the case of CZBi/SBA-16 and CZ/SBA-16, the peaks intensities of (110) and (200) [37, 38] were slightly decreased, indicating a slight loss of periodicity of the mesopores in SBA-16. In addition, since the peaks shifted to higher angles, a decrease of pore diameter of SBA-16 was assumed. These results also suggest that CZBi or CZ were loaded into the mesopores of SBA-16.

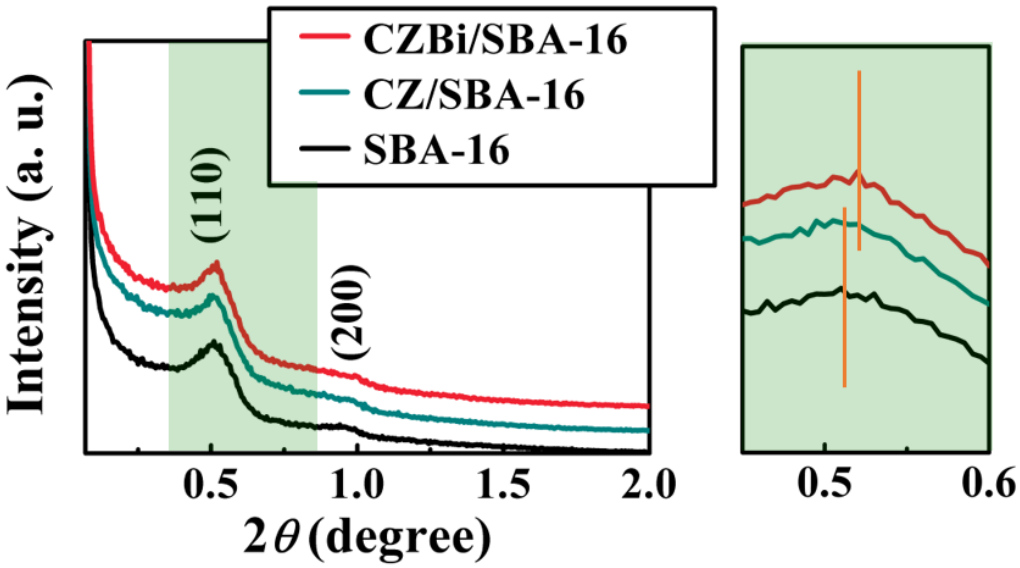

Figure 3.4. SAXS patterns of CZBi/SBA-16, CZ/SBA-16, and SBA-16.

Figure 3.5 shows the results of the Rietveld refinement of the XRD pattern for CZBi/SBA-16 and CZ/SBA-16. For the Rietveld analysis, I used the pattern of the SBA-16 support as a background and the occupations of each cation were the results estimated from the XRF. From the Rietveld analysis for CZBi/SBA-16, all the diffraction peaks were indexed as a single-phase for cubic fluorite structure of CZBi, and no impurity phases were observed. Also, for CZ/SBA-16, the diffraction peaks were indexed as only a cubic fluorite-type structure.

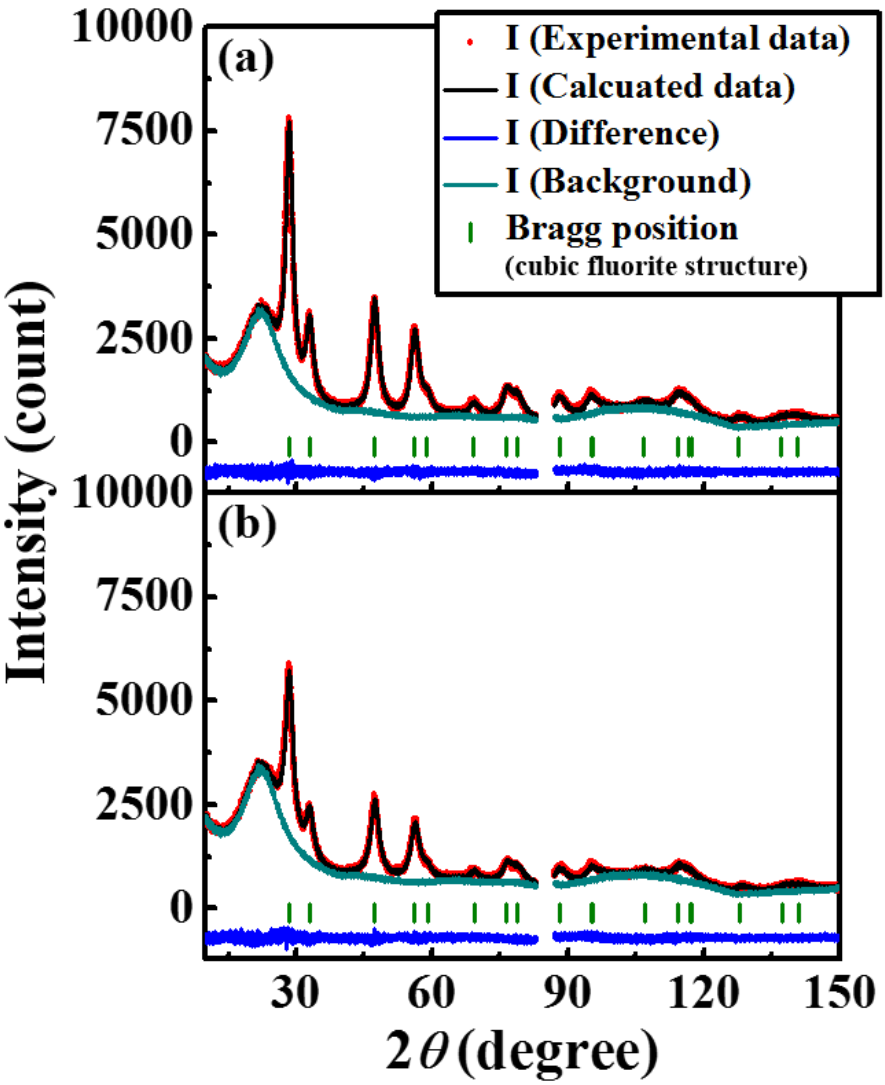

Figure 3.5. Results of the Rietveld analysis for (a) CZBi/SBA-16 and (b) CZ/SBA-16.

The structural parameters of cubic fluorite-type structure are summarized in Table 3.1. The lattice expansion for the fluorite-type structure (CZBi: 0.5438 nm, CZ: 0.5422 nm) was observed by introducing Bi ions, because the average cationic radius at the 4*a* site in the CZBi lattice (0.098 nm) is larger than that of the CZ lattice (0.095 nm). The average cationic radii were calculated from the occupations and ionic radii of each cation: 0.097 nm for Ce, 0.084 nm for Zr, and 0.117 nm for Bi (coordination number = 8) [41]. By introducing Bi ions into the CZ lattice, the oxygen occupation (0.886) decreased as comparison to that of CZ (0.921), due to lower-valent of Bi^{3+} ion into the CZ lattice, thereby indicating that an additional oxygen vacancy was formed.

Table 3.1. Structural parameters of cubic fluorite-type phase for the CZBi/SBA-16 and CZ/SBA-16

Sample	Lattice Parameter (nm)	Atom	Wyckoff Position	Occupation	*x*	*y*	*z*	*B*(Å^2)
CZBi/SBA-16	0.5428(1)	Ce	4*a*	0.67	0	0	0	1
		Zr	4*a*	0.18	0	0	0	1
		Bi	4*a*	0.15	0	0	0	1
		O	8*c*	0.886(4)	1/4	1/4	1/4	1
Space group: $Fm\bar{3}m$, R_{wp} = 3.83%, S = 1.36								
CZ/SBA-16	0.5422(1)	Ce	4*a*	0.85	0	0	0	1
		Zr	4*a*	0.15	0	0	0	1
		O	8*c*	0.921(4)	1/4	1/4	1/4	1
Space group: $Fm\bar{3}m$, R_{wp} = 4.00%, S = 1.38								

TEM and electron diffraction images of CZBi/SBA-16 are shown in Figure 3.6. The CZBi/SBA-16 catalyst possessed a regular arrangement of pores with a diameter of ca. 12 nm. Although it is difficult to distinguish between CZBi and SBA-16 on the TEM image, the electron diffraction image was clearly indexed to the same positions as the cubic fluorite-type structure of CZBi. These results demonstrate that CZBi was well dispersed into the mesopores of SBA-16 and show good agreement with the results of N_2 adsorption-desorption isotherms, pore size distribution, XRD, and SAXS described above.

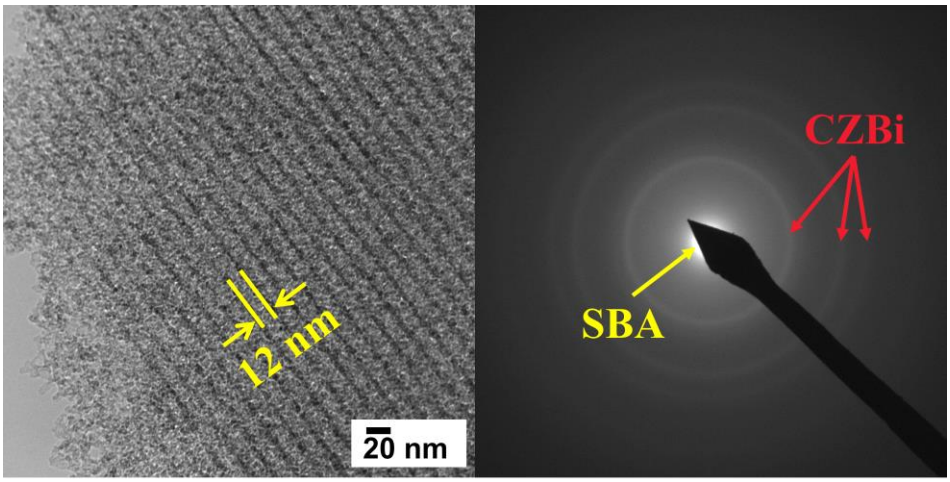

Figure 3.6. TEM and electron diffraction images of CZBi/SBA-16.

Figure 3.7 shows the removal percentages for BPA on the CZBi/SBA-16, SBA-16, and CZ/SBA-16 under atmospheric pressure for 3 h. For comparison, the result reported for the Ag/CZ catalyst [22] is also depicted. The SBA-16 support showed the removal performance of BPA. This was due to adsorption on and in the mesoporous structure with a large surface area of SBA-16 (787 m^2 g^{-1}). After CZ or CZBi loading, the removal percentages were increased. Therefore, the catalytic removal process was assumed to have proceeded successfully even for the catalyst without precious metal. Especially, for the CZBi/SBA-16 catalyst, the highest catalytic activity was realized and the removal percentage of BPA reached up to 82% due to the increase of the oxygen release property by introducing Bi^{3+} ions into the CZ lattice. Moreover, the CZBi/SBA-16 catalyst exhibited higher removal percentage even at moderate condition (under atmospheric pressure at 80°C) as compared to reported Ag/CZ, which exhibited 76% of removal percentage under 20 atm at 160°C.

Products after the reaction using the CZBi/SBA-16 catalyst was investigated by the GC-MS. Although quantitative analysis is difficult due to the overlap of peaks in GC, some oxidative decomposition products were detected, such as *tert*-amyl alcohol and ethyl formate, indicating that oxidation reaction might occur on the catalyst.

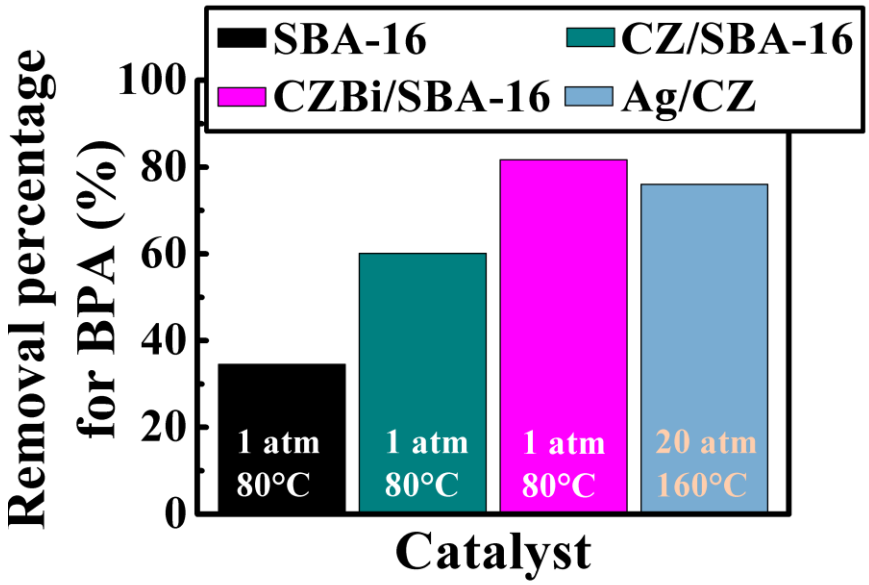

Figure 3.7. The removal percentage for BPA on SBA-16, CZ/CZB-16, CZBi/SBA-16, and Ag/CZ [22] (3 h).

To examine reusability, the catalyst was reused for the catalytic oxidation of BPA without being washed. The reusabilities were identified by the R_{reused}/R_{fresh} ratio (R_{fresh} : removal percentage with fresh catalyst, R_{reused} : removal percentages with reused catalyst), and the results are shown in Figure 3.8. For SBA-16, the catalytic activities after consecutive usage were obviously decreased, because the BPA adsorbed in the first cycle impeded further adsorption. On the other hand, in the case of CZBi/SBA-16 catalyst, the catalytic activities were almost maintained with high values over 90%, because almost of BPA was removed by the oxidation reaction. These results indicate that the CZBi/SBA-16 catalyst possessed the high reusability and the catalytic reaction proceeded continuously.

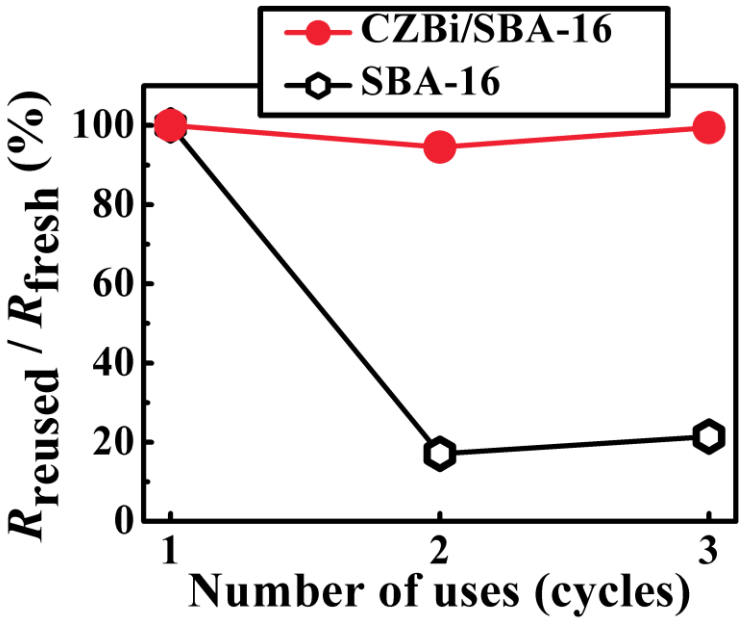

Figure 3.8. Reaction cycle dependences of the removal percentage for BPA on CZBi/SBA-16, and SBA-16 (1atm, 3 h, 80°C).

3.4. Conclusions

In this chapter, the CZBi/SBA-16 catalyst without precious metal of Pt was synthesized for efficiently removal of the refractory hazardous organic compound of BPA in water under moderate condition.

CZBi was successfully dispersed in and/or on the regularly arranged mesopores of SBA-16 by an impregnation process. For the CZBi/SBA-16 catalyst, removal percentage was reached up to 82% after the reaction for 3 h at moderate condition (atmospheric pressure, 80°C), and the removal degree is higher than that reported for Ag/CZ (76%) under 20 atm at 160°C. Additionally, the catalyst possessed high reusability.

Summary

In the study of this thesis, the development of novel catalysts that can be realized high catalytic removal property for hazardous and refractory organic compounds in water under moderate condition without the supply of any additives or UV irradiation by introducing high oxygen release and storage abilities of oxides with rare earth was described.

The results obtained through this study are summarized as follows:

Chapter 1

To efficient removal for the hazardous organic compound of acetaldehyde in water under moderate condition, I designed the catalyst composed with $Ce_{0.68}Zr_{0.17}Sn_{0.15}O_2$ having high oxygen release and storage abilities as promotor, metallic Pt with of the high catalytic oxidation activity, and γ-Al_2O_3 with the high specific surface area as a support.

The Pt/CZSn/ γ-Al_2O_3 catalyst was successfully synthesized by impregnation and co-precipitation processes. The catalyst exhibited high catalytic activity under atmospheric pressure at 0°C for acetaldehyde removal. The catalyst fully removed acetaldehyde in water by oxidation reaction after the reaction for 8 h.

Chapter 2

For efficiently remove of the refractory hazardous organic compound of 1,4-dioxane in water under moderate condition, I increase the catalytic active sites using SBA-16 as a support which possessed the considerably high specific surface area. In addition, I selected not only CZSn but also CZBi which

also possess high oxygen release and storage abilities as a promoter, and the Pt/CZSn/SBA-16 and Pt/CZBi/SBA-16 catalysts were prepared.

The Pt/CZSn and Pt/CZBi were successfully dispersed in and/or on the regularly arranged mesopores of SBA-16 by impregnation and co-precipitation processes. The novel Pt/CZSn/SBA-16 and Pt/CZBi/SBA-16 catalysts possessed high surface areas and exhibited high catalytic activities for 1,4-dioxane removal under atmospheric pressure at 80°C without any supply of additives. Removal percentages were reached to 69% and 59% after the reaction for 4 h on Pt/CZSn/SBA-16 and Pt/CZBi/SBA-16 respectively. Furthermore, the oxidation of 1,4-dioxane proceeded completely to harmless carbon dioxide and water without byproducts. The highest catalytic activity was obtained on the Pt/CZSn/SBA-16 catalyst, and it possessed the high reusability.

Chapter 3

In chapter 3, in order to remove refractory hazardous organic compound of BPA efficiently, CZBi/SBA-16 without Pt was synthesized and investigated for catalytic removal of BPA.

CZBi was successfully dispersed in and/or on the regularly arranged mesopores of SBA-16 by an impregnation process. The CZBi/SBA-16 catalyst possessed the high surface area and exhibited the high catalytic activity under atmospheric pressure at 80°C and removal percentage was reached to 82% after the reaction for 3 h. Additionally, the catalyst possessed high reusability.

References

[1] K.H. Kim, S.K. Ihm, *J. Hazard. Mater.*, **186**, 16-34 (2011).

[2] Tawfik A. Saleh, M.A. Gondal, Q.A. Drmosh, Z.H. Yamani, A. AL-yamani, *Chem. Eng. J.*, **166**, 407-412 (2011).

[3] L.N. Vandenberg, R. Hauser, M. Marcus, N. Olea, W.V. Welshons, *Reprod. Toxicol.*, **24**, 139-177 (2007).

[4] T. Geens, D. Aerts, C. Berthot, J.P. Bourguignon, L. Goeyens, P. Lexomte, G. Maghuin-Rogister, A.M. Pironnet, L. Pussemier, M.L. Scippo, J.V. Loco, A. Covaci, *Food Chem. Toxicol.*, **50**, 3725-3740 (2012).

[5] T.K.G. Mohr, *Environmental investigation and remediation: 1,4-dioxane and Other Solvent Stabilizers*, Santa Clara Valley Water District, San Jose, CA, USA (2011).

[6] L.A. Schaider, R.A. Rudel, J.M. Ackerman, S.C. Dunangan, J.G. Brody, *Sci. Total Environ.*, **468-469**, 384-393 (2014).

[7] C.D. Adams, P.A. Scanlan, N.D. Secrist, *Environ. Sci. Technol.*, **28**, 1812-1818 (1994).

[8] H. Melcer, G. Klečka, *Water Environ. Res.*, **83**, 650-666 (2011).

[9] P. Westerhoff, Y. Yoon, S. Snyder, E. Wert, *Environ. Sci. Technol.*, **29**, 6649-6663 (2005).

[10] S. Chitra, K. Paramasivan, M. Cheralathan, P.K. Sinha, *Environ. Sci. Pollut. Res.*, **19**, 871-878 (2012).

[11] W. Fan, Y. Kubota, T. Tatsumi, *ChemSusChem*, **1**, 175-178, (2008).

[12] H. Barndõk, L. Cortijo, D. Hermosilla, C. Negro, Á. Blanco, *J. Hazard. Mater.*, **280**, 340-347 (2014).

[13] M. Beborde, S. Rabouan, P. Mazellier, J.P. Duguet, B. Legube, *Water Res.*, **42**, 4299-4308 (2008).

[14] E. Nikfar, M.H. Dehghani, A.H. Mahvi, N. Rastkari, M. Asif, I. Tyagi, S. Agarwall, V.K. Gupta, *J. Mol. Liq.*, **213**, 332-338 (2016).

[15] I. Ioan, S. Wilson, E. Lundanes, A. Neculai, *J. Hazard. Mater.*, **142**, 559-563 (2007).

[16] M. Bistan, T. Tišler, A. Pintar, *Ind. Eng. Chem. Res.*, **51**, 8826-8834 (2012).

[17] T. Vescovi, H.M. Coleman, R. Amal, *J. Hazard. Mater.*, **182**, 75-79 (2010).

[18] H.S. Son, S.B. Choi, E. Khan, K.D. Zoh, *Water Res.*, **40**, 692-698 (2006).

[19] H. Barndõk, D. Hermosilla, C. Han, D.D. Dionysiou, C. Negro, Á. Blanco, *Appl. Catal. B: Environ.*, **180**, 44-52 (2016).

[20] N.K. Youn, J.E. Heo, O.S. Joo, H. Lee, J. Kim, B.K. Min, *J. Hazard. Mater.*, **177**, 216-221 (2010).

[21] K. Sei, K. Miyagaki, T. Kakinoki, K. Fukugasako, K. Inoue, M. Ike, *Biodegradation*, **24**, 665-674 (2013).

[22] A. Heponiemi, S. Azalim, T. Hu, U. Lassi, *Top. Catal.*, **58**, 1043-1052 (2015).

[23] K. Yasuda, A. Yoshimura, A. Katsuma, T. Masui, N. Imanaka, *Bull. Chem. Soc. Jpn.*, **4**, 522-526 (2012).

[24] A. Holmgren, D. Duperz, B. Andersson, *J. Catal.*, **182**, 441-448 (1999).

[25] N. Imanaka, T. Masui, K. Koyabu, K. Minami, T. Egawa, *Adv. Mater.*, **19**, 1608-1611 (2007).

[26] G. Balducci, J. Kašpar, P. Fornasiero, M. Graziani, *J. Phys. Chem. B*, **102**, 557-561 (1998).

[27] C. Cau, Y. Guari, T. Chave, J. Larionova, P. Pochon, S. Nikitenko, *J. Phys. Chem. C*, **117**, 22827-22833 (2013).

[28] H.C. Yao, Y.F.Y. Yao, *J. Catal.*, **86**, 254-265 (1984).

[29] J. Kašpar, P. Fornasiero, M. Graziani, *Catal. Today*, **50**, 285-298 (1999).

[30] T. Montini, M. Melchionna, M. Monai, P. Fornasiero, *Chem. Rev.*, **116**, 5987-6041 (2016).

[31] M. Batzill, U. Diebold, *Prog. Surf. Sci.*, **79**, 47-154 (2005).

[32] A.A. Mohamed, A.T. Mubrak, Z.M.H. Marestani, K.F. Fawy, *Talanta*, **74**, 578-585 (2008).

[33] T. Masui, H. Imadzu, N. Matsuyama, N. Imanaka, *J. Hazard. Mater.*, **176**, 1106-1109 (2010).

[34] S. Budavari, M.J. O'Neil, A. Smith, *The Merck Index*, ed., P.E. Heckelman. 11th edition, Merck & Co., Inc., Rahway, NJ, USA (1989).

[35] M.J. Zenker, R.C. Borden, M.A. Barlaz, *Environ. Eng. Sci.*, **20**, 426-432 (2003).

[36] A. Abe, *Sci. Total. Environ.*, **227**, 41-47 (1999).

[37] S. Zuo, G. Liu, J. Tong, C. Qi, *Appl. Catal. A: Gen.*, **467**, 1-6 (2013).

[38] D. Zhao, Q. Huo, J. Feng, B.F. Chmelka, G.D. Stucky, *J. Am. Chem. Soc.*, **120**, 6024-6036 (1998).

[39] H. Yotou, T. Okamoto, M. Ito, T. Sekino, S.I. Tanaka, *Appl. Catal. A: Gen.*, **458**, 137-144, (2013).

[40] F. Izumi, K. Momma, *Solid State Phenom.*, **130**, 15-20 (2007).

[41] R.D. Shannon, *Acta Crystallogr. Sect. A*, **32**, 751-767 (1976).

[42] Y. Wei, J. Liu, Z. Zhao, C. Xu, A. Duan, G. Jiang, *Appl. Catal. A: Gen.*, **453**, 250-261 (2013).

[43] N. Yamaguchi, N. Kamiuchi, H. Muroyama, T. Matsui, K. Eguchi, *Catal. Today*, **164**, 169-175 (2011).

[44] T. Matsui, T. Okanichi, K. Fujiwara, K. Tsutsui, R. Kikuchi, T. Takeguchi, K. Eguchi, *Sci. Technol. Adv. Mater.*, **7**, 524-530 (2006).

[45] K. Yasuda, M. Nobu, T. Masui, N. Imanaka, *Mater. Res. Bull.*, **45**, 1278-1282 (2010).

Acknowledgements

The author would like to express his heartfelt gratitude to professor Dr. Nobuhito Imanaka, Division of Applied Chemistry, Graduate School of Engineering, Osaka University, for his continuous guidance, invaluable suggestions, and science encouragement throughout the work. The author is very grateful to Dr. Naoyoshi Nunotani, Division of Applied Chemistry, Graduate School of Engineering, Osaka University, for his continuous guidance and stimulating discussion for carrying out this work. The author is also indebted to Professor Dr. Shinji Tamura, Division of Applied Chemistry, Graduate School of Engineering, Osaka University, for his helpful suggestions and heartfelt advice.

The author is deeply grateful to Professor Dr. Hiroshi Uyama, Division of Applied Chemistry, Graduate School of Engineering, Osaka University, and Professor Dr. Takahiro Kozawa, the institute of Scientific and Industrial Research (Division of Applied Chemistry, Graduate School of Engineering), Osaka University, for reviewing this these and giving their valuable comments.

Special thanks should be given to author's co-workers, Mr. Minchan Jeong, Mr. Naoki Moriyama, Mr. Abdul Rohman Supandi, and Mr. Kenji Matsuo for their helpful assistance and support in the course of the work, and members of the research group under direction of Professor Dr. Nobuhito Imanaka, Osaka University.

The author would like to thank to Professor Dr. Dong Sik Bae of Changwon National University in South Korea for his helpful comments and encouragement.

Finally, the author would like to deeply thank to his parents Mr. Jae Hwan Choi and Mrs. Kyung Min Kwon, and brother Han Gyu Choi for their encouragement, continuous understanding, and perpetual supports.